

Spatial interactions reveal differing natures of first-order and higher order motion processing

Peter Meilstrup

A dissertation submitted
in partial fulfillment of the
requirements for the degree of

Doctor of Philosophy

University of Washington
2013

Reading Committee:
Michael Shadlen, chair
Ione Fine
Ric Robinson
John Palmer

Program Authorized to Offer Degree:
Graduate Program in Neurobiology and Behavior

1 Introduction

Accurate motion perception is essential for visually guided movement; complex behaviors such as chasing prey, escaping predators, running while avoiding obstacles, or catching a thrown ball require that an organism be able to rapidly determine the position and velocity of a moving object, and to anticipate its trajectory through space. Psychological research on motion perception has established that local and global motion are processed by separate mechanisms, an idea that dates back to Wertheimer’s phenomenological distinction between the sensations elicited by faster “phi” and slower “beta” stimuli (Wertheimer 1912, 2012; Steinman et al., 2000). The goal of this thesis is to examine how separate mechanisms contribute to a unified perception of motion.

It is generally believed that there are multiple classes of motion mechanisms. One of these, the FIRST-ORDER motion mechanism, seems to respond to local spatiotemporal correlations in luminance contrast, at relatively short timescales and in small regions of space. It is generally agreed that the first-order motion mechanism originates with the direction selective response of cells in area V1. Classic models of first-order motion detection use linear filters tuned to certain combinations of spatial and temporal frequencies, with the outputs of several such filters being combined nonlinearly (Adelson and Bergen, 1985; Watson and Ahumada, 1985). With some embellishments, the responses observed from cells in area V1 are largely compatible with this type of model (Movshon et al., 1978; Rust et al., 2005; Touryan et al., 2005; Chen et al., 2007), and models of higher order processing can be built on this basis (Graham, 2011). Moreover, the size and bandwidth of motion sensing channels inferred from psychophysical measurements are similar to those observed of V1 neurons (Anderson and Burr, 1987, 1989; Banks et al., 1991; Anderson et al., 1991; Watson and Turano, 1995).

However, these first-order mechanisms cannot by themselves fully explain human motion perception. For example, perceiving visual motion does not necessarily require moving features to differ in mean luminance from the background, and does not require motion energy in the Fourier domain. Many forms of HIGHER-ORDER motion stimuli have been constructed that would not be consistently detectable to first-order mechanisms, but these stimuli still elicit strong sensations of movement (Derrington and Badcock, 1985; Chubb and Sperling, 1988; Zanker, 1990). These higher order stimuli have been used to provide evidence for and characterize motion sensing systems separate from the first-order mechanisms. They have been constructed variously by modulations in contrast, texture, or other stimulus features, but generally involve the change in position, over time, of some feature in the image (Lu and Sperling, 1995).

One possible reason for having multiple motion systems is that first-order motion signals are not always a reliable indication of the veridical motion of an object. In a complicated visual world, motion can come from many sources, and accurate perception of the movement of objects requires disambiguating motion signals attributable to the object from irrelevant motions in the background or of other objects. Consider the task of trying to track the movement of a zebra among a background of waving grass. One challenge this task presents is that

a motion energy sensor with a limited receptive field size will report the component of the zebra’s motion orthogonal to its stripes, rather than the veridical motion of the zebra, an instance of the so-called “aperture problem”(Illdreth and Ullman, 1982; Adelson and Movshon, 1982) Combining the component motion signals from V1 cells spanning a larger area might allow disambiguation of the true velocity. This extraction of first-order pattern motion from component motion appears to be one of the roles of visual area MT (Movshon et al., 1985; Simoncelli and Heeger, 1998; Rust et al., 2006). However, this computation of pattern motion cannot completely explain motion perception either, as it introduces a problem in the loss of spatial selectivity. If motion information is pooled over a large area, the motion of the background grass will create a subset of the pooled signals that are substantially incorrect; an MT cell analyzing the motion of the zebra will mix together signals from the zebra’s stripes with signals from the grassy background.

A related problem is that in computing an accurate velocity of a pattern discards information about the location of the stimulus. The computation in MT resolves texture motion but appears to lose information about where the motion is occurring within the large MT receptive fields (Majaj et al., 2007). This is puzzling because often the ostensible purpose served by motion perception to track and anticipate the change in position of a physical object. Consider tracking an animal moving through obscuring tall grass, or watching waves pass over choppy water. The stalks of grass, or the foam and texture on the water, do not progressively change position; they only oscillate in place as the movement passes under them. A computation based on first-order or pattern motion would generally track the oscillation of the surface texture rather than that of the underlying movement. However it is the underlying movement that is more relevant, and often dominates the perception of motion.

Literature on visual motion processing has drawn many different demarcations between types of motion. Various papers have discussed first-order versus second-order, short-range vs. long-range, local vs. global, textural versus figural, and so on, based on particular distinctions drawn among stimulus properties or proposed mechanisms (Nishida, 2011). For the purposes of this thesis I will also have to pick a demarcation. The tension in the problem of motion perception alluded to by the examples of animals in the grass and waves on the water is that of combining information about first-order signals, for which we are reasonably confident of the mechanism, with information about spatial position. This information about the changing spatial position of an object is what I will be referring to as higher-order motion. Tracking the zebra might require integrating locally occurring first-order motion signals motion signals over space and time in a way that is consistent with the global change in position of an object, while discarding adjacent signals that are inconsistent with the object’s trajectory.

There is evidence that perception of higher order motion stimuli may have a separate neural substrate from first-order motion. For example, adding higher order motion to a display does not appear to change the threshold of detection for first-order motion, and any effects in the other direction are weak and non-

selective (Edwards and Badcock, 1995; Nishida et al., 1997; Cassanello et al., 2011, but see Hedges et al., 2011). When differing first-order and higher order components are present in a stimulus, the motion after-effect is always directed against the first-order component, whereas perception of the stimulus is often determined by the higher order component (Derrington and Badcock, 1985; Chubb and Sperling, 1989; Nishida and Sato, 1992). Neuropsychological evidence suggests a double dissociation between first-order and higher-order motion processing deficits in a number of patients (Vaina and Cowey, 1996; Vaina and Soloviev, 2004), suggesting that different motion mechanisms may have anatomically distinct pathways. Another difference between first-order and higher-order stimuli that suggests different mechanisms is that the former seems to be capable of tracking objects through a feature object over distances larger than what can be achieved through individual local filters. “Long-range” apparent motion stimuli span a distance greater than the classical receptive field size in V1, eliciting sensations of motion without explicit direction selective activity in V1.

Interestingly, the physiological substrate of higher-order motion processing is still unclear. Cortical area MT (or somewhere downstream) has been proposed as a locus of integration between motion and position information (Nishida and Johnston, 1999; McGraw et al., 2004; Mather and Pavan, 2009). While the receptive fields of cells in cortical areas MT and MST are large enough that they might be able to integrate information about objects that change position, recordings of these cells find their responses dominated by first-order motion and showing little to no selectivity to higher-order, position-defined motion, even when the higher-order motion corresponds better to the experience of viewing these stimuli (Livingstone et al., 2001; Ilg and Churan, 2004; Hedges et al., 2011). So while signals present in MT have an influence on perceived position, MT does not itself appear to track perceived position. Despite the fact that these two motion systems clearly both contribute to determining the appearance of the moving world, the question of whether and how they interact to produce a single coherent percept of motion remains open (Nishida, 2011). In this thesis I examine the combination of these two types of motion using a simple display that contains first-order and higher-order components whose direction of motion can be independently manipulated.

Figure 1 provides examples of first order and higher order motion, and how they can interact. The elements are Gabor-like stimuli that can be understood as a carrier grating windowed by a spatial envelope. The envelope moves independently of the carrier, so that the *carrier* provides *first order motion* while the *envelope* produces *higher order motion*. Figure 1A illustrates the difference between first-order and higher-order motion. On the left is a single element with carrier (i.e. first-order) motion but no envelope motion. On the right side, the element has envelope motion but its carrier motion is balanced. The higher order motion on the right is seen as a clear progressive change in position, while the first order motion on the left has an appearance more like a flicker. (The position of the element on the left does appear to shift slightly, opposite its first-order motion. This is an example of motion-induced position shift; De Valois

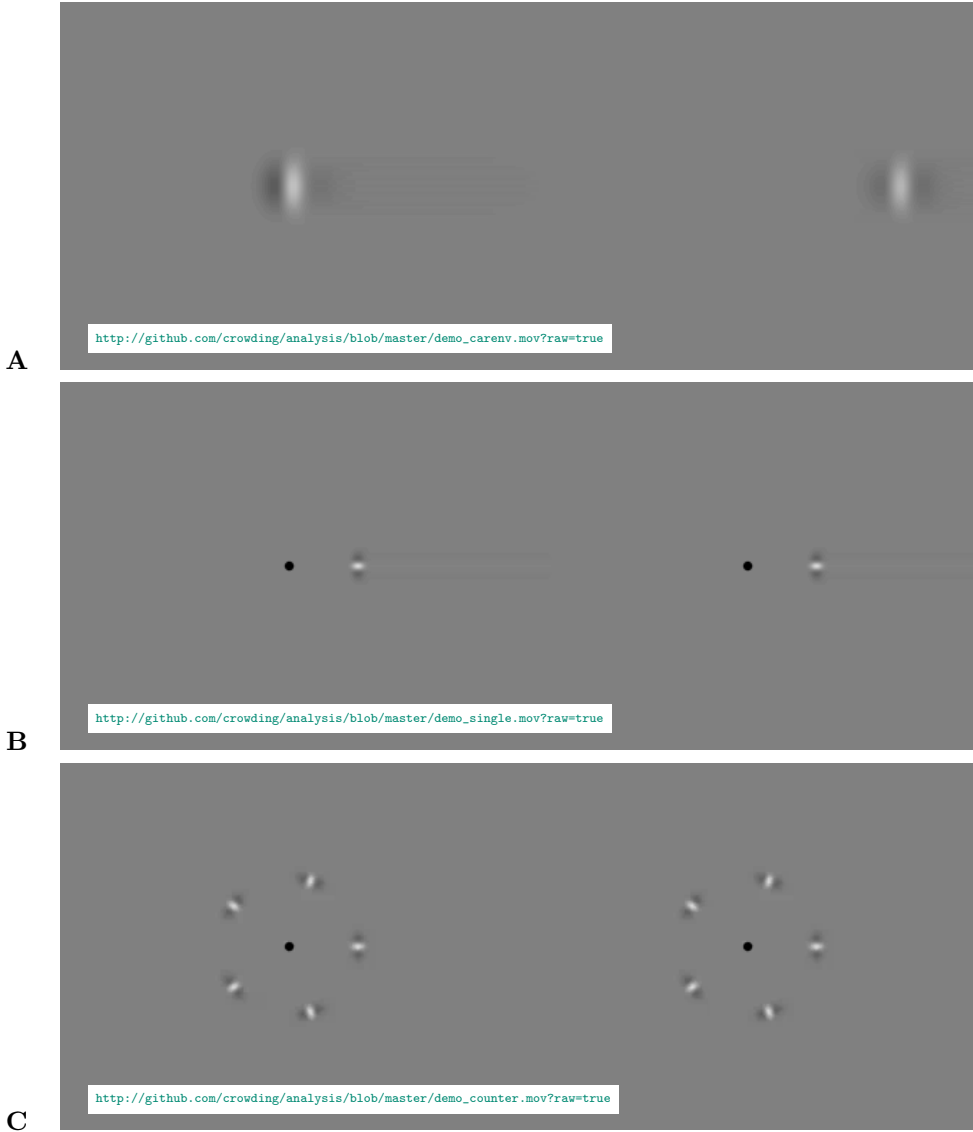


Figure 1: Examples of carrier/envelope stimuli. **A.** At left, an element contains carrier (first-order) motion in the absence of higher order motion. At right, an element whose carrier motion is balanced, but the envelope moves (higher order motion.) **B.** Single motion elements, moving in circles. At left, the carrier motion is opposite the envelope motion. At right, the carrier motion is in the same direction as the envelope motion. **C.** Five elements, each identical to the single element in subfigure B, distributed around each fixation point. When elements are closely spaced, there is an eccentricity-dependent change in appearance. The appearance of the wheel on the left (with opposing carrier and envelope motions) changes depending on where the eyes fixate.

and De Valois, 1991; Ramachandran and Anstis, 1990).

In [Figure 1B](#), elements have both carrier and envelope motion. On the left, the carrier and envelope components move in the same direction; on the right the carrier and envelope motions are in opposite directions. Full details of the construction of this display are given in [Section 3](#). [Figure 1C](#) is the same but with five elements around each fixation point.

When elements with combined envelope and carrier motions are viewed in isolation, as in [Figure 1B](#), the appearance of the direction of motion follows the motion of the envelope, and not strongly affected by the direction of the carrier. The carrier motion does cause a change in the sense of “smoothness,” with conflicting motion having a more jittery appearance, but does not strongly affect the apparent direction or even the apparent speed of the motion. However, in [Figure 1C](#), when multiple elements are placed in proximity, but not overlapping, the apparent motion depends on whether the stimulus is viewed centrally or peripherally. When the five-element ring on the left is viewed centrally, the apparent direction of motion is consistent with the envelope. When the same element ring is viewed in the periphery, the apparent direction of rotation matches that of the carrier. If an observer maintains attention on the leftward ring, which has carrier and envelope in conflict, while moving their eyes so as to move the stimulus from central to peripheral vision, the apparent motion may appear to reverse in concert with the eye movement.

From this demonstration it appears that having more than one element in proximity affects how first-order and higher-order motion are combined. That the appearance changes with retinal eccentricity of the stimulus suggests that the range of spatial interaction scales with retinal eccentricity. A plausible explanation could be that the presence of flanking objects limits the ability to see movement of the envelope, thereby allowing the carrier motion to determine the percept; that is, crowding ([Levi, 2008](#); [Pelli, 2008](#)) may be affecting how first-order and higher-order motion are combined.

In this thesis I examine how first-order and higher order mechanisms interact in forming an overall perception of motion. In [Experiment 1](#) I quantify how element spacing determines the sensitivity to first-order and higher order motions and present a simple model to capture the results, wherein first-order and higher-order motion signals are processed separately and combined at a decision stage. In [Experiment 2](#) we vary the number of elements independently of the spacing of targets and determine that first-order motion sums inputs over a large area, while higher order motion perception is sensitive to the spacing between elements and flankers.

2 Demonstrations and Subjective Observations

A model of visual processing of this class of stimuli responses will need to account for changes in the direction of apparent motion. When elements are isolated, the apparent direction of motion follows that of the envelopes; when multiple elements are placed in proximity, the direction of apparent motion changes to agree with that of the carrier. I will proceed to quantify this reversal effect in subsequent sections. In order to do so I asked naïve observers to make binary classifications of their impressions of the overall direction of motion (clockwise or counterclockwise.) However, binary responses collapse together a number of perceptual qualities, so that these simple direction judgments do not fully capture the appearance of these stimuli.

Below are three demonstrations that place the fixation point in the center of the screen and the moving elements on a circle of constant eccentricity. The motion of the individual elements is the same in each demo; only the spacing and number of elements changes. These movies are arranged to loop, however the psychophysics I will discuss in subsequent sections is based on brief (500ms) presentations of motion.

[Figure 2](#) shows six elements, so the spacing between elements is $1.04e$ measured circumferentially. In this demonstration the carrier motion is clockwise and the envelope motion is counterclockwise. For all observers I have shown this stimulus to, the perceived direction of motion is clockwise, in agreement with the envelope motion. This illustrates that higher order motion can be clearly seen in the periphery, and that at these wide element spacings the envelope motion dominates the perception. Compared to other stimuli it is relatively difficult to tell the direction of motion of the carrier, so we could say that the envelope motion “captures” the carrier motion ([Hedges et al., 2011](#)). For the largest values of carrier strength, (for these demonstrations, the carrier strength C as defined in [General Methods](#) is 100%,) the carrier motion might appear as a “wind” which overlays the moving envelopes, somewhat similar to the appearance of a low-contrast moving grating superposed on a stationary pedestal grating ([Lu and Sperling, 2001](#)). Incidentally, when carrier motions are directed opposite to envelope motion, as can be seen in [Figure 1](#), the elements appear to have more flicker, and the perceived motion, while agreeing in direction with the envelope, seems less smooth.

As the number of elements in the display increases and the spacing between elements decreases, the appearance of the motion changes. The demonstration in [Figure 3](#) increases the number of elements to 16; the spacing between elements is $0.39e$, which seems close to the “critical spacing” for many observers. Generally the carrier motion becomes more visible and observers begin to equivocate in their reports of perceived motion direction. The perception is a mixture of both carrier and envelope motions, but the form of this mixture can take on several different appearances. Observers viewing stimuli near the critical spacing described a number of different qualitative impressions of the stimulus:

- Transparent motion, in which different layers seemed to slide over each

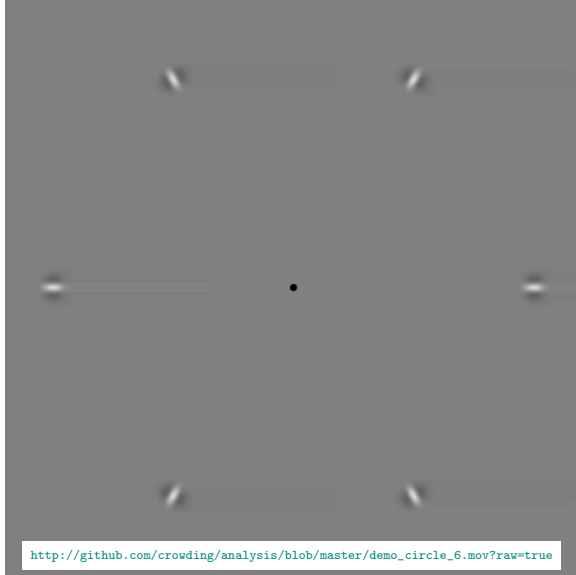


Figure 2: An example motion stimulus similar to those used in my experiments. There are six elements, with the carrier motion clockwise and the envelope counterclockwise. The envelope motion dominates the subjective appearance.

other in opposite directions;

- Windowed motion, in which the elements appear to be rotating aperture through which a moving background is seen.
- Motion that changes direction over time. In these cases the immediate perception was usually in agreement with the carrier motion while the later percept was in agreement with the envelope motion.
- A non-uniform appearance where one side of the wheel appears to move one direction and the other side in the other direction.
- A few isolated elements move in agreement with the envelope motion and can be attentively tracked, but non-attended regions of the wheel seem to move in the opposite direction.

The subjective speed of the motion can change as spacing is brought near critical; if carrier motion opposes envelope motion, the perceived speed of the stimulus reaches a minimum at a certain spacing, being faster in the direction of envelope motion when spacing is larger and faster in the direction of carrier motion when spacing is smaller.

Some observers saw motion directions in agreement with the carrier immediately after stimulus onset which then changes to be more in agreement with

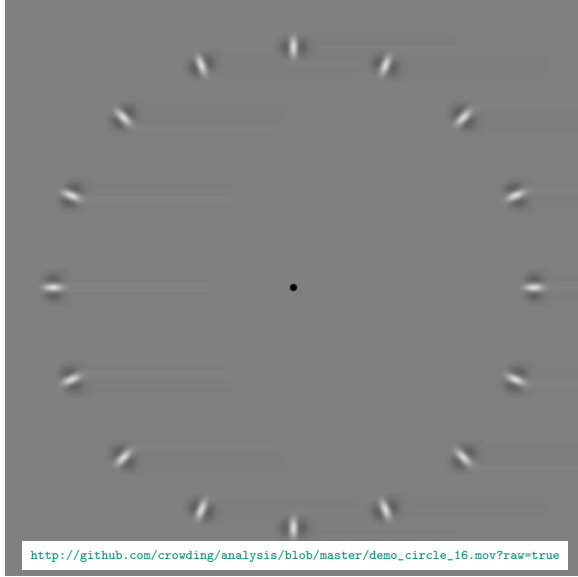


Figure 3: Same stimulus as [Figure 2](#) with sixteen elements. The appearance may be a mixture of carrier and envelope motions.

the envelope motion. For this reason I asked observers in [Experiment 1](#) to respond within a restricted time window. Observers often reported cases where they gave a mistaken response (i.e. they gave a response but their perception of motion changed after they had committed to the response.)

One perceptual phenomenon that did *not* seem to occur is bistability. Both the carrier and envelope motions are individually consistent with a global rotation of the display around the fixation point, so that we might have anticipated perceptions exclusively consistent one rigid movement or the other ([Anstis and Kim, 2011](#)). However, the appearances of critically spaced stimuli tended to reflect a mixture of two motions rather than one overriding motion, and there was never the spontaneous all-at-once switch that occurs for perceptually bistable stimuli.

The third demonstration in [Figure 4](#) has 22 elements spaced at $0.29e$. For most observers it becomes difficult to see the envelope motion at this density especially at short viewing durations. When elements are this closely spaced the overall impression is of motion in the direction of the carrier. There is not as much of the appearance of two separate motions. However, the amount of subjective flicker does appear to increase when carrier motion is incongruent with envelope motion.

While I did not describe the stimulus construction in detail to naïve observers, all observers after having practiced at the task employed in [Experiment 1](#) commented spontaneously on the two forms of motion being employed. More

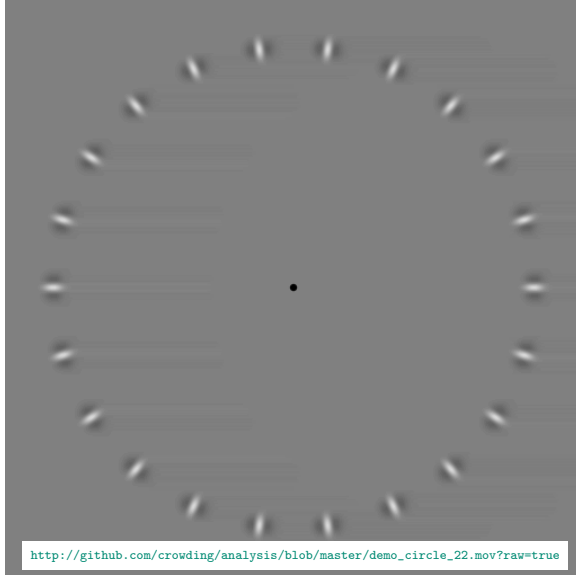


Figure 4: A stimulus with 22 identical elements. For most observers, carrier motion dominates the appearance.

than one observer when commenting on the stimuli called the envelope morion “real” and the carrier motion “fake.” However the two motions are not equally salient or distinguishable in all conditions; the carrier motion appears less salient when spacing is wide, with few elements on screen, and envelope motion is more difficult to discern in the contrary situation. Motion after-effects appear to always be directed opposite the carrier motion regardless the spacing or the envelope motion.

There seems to be some individual variation as to how relatively strong carrier and envelope motions are. For some observers I was able to find a configuration of carrier strength, envelope motion, and spacing which I would perceive as clearly being clockwise but the observer would perceive as counterclockwise. While appearance was affected by carrier motion, it was not always affected in the *direction* of carrier motion; I sometimes found that adding carrier motion in one direction to a stimulus prompted a report that the stimulus was now moving in the opposite direction to the change. Sometimes I could even find a stimulus where both the carrier and envelope motion were clockwise but whose appearance was counterclockwise. An effort at modeling the processes underlying this behavior will therefore have to capture this individual variation and the apparent nonlinearity in carrier motion perception.

There are too many stimulus parameters to explore the entire configuration space exhaustively, but I can report some impressions as to the robustness of the appearance of the stimulus. In particular I wondered whether the density-driven

reversal of apparent motion was robust to changes in stimulus properties such as element size and eccentricity. A scaling of critical spacing with eccentricity and robustness of critical spacing against changes in target size have been proposed as two diagnostic tests of visual crowding (Pelli, 2008).

Adjusting the spacing from wide to narrow by adding more elements revealed a point at which the appearance of motion changed from envelope-dominated to carrier-dominated. I noted the spacing (or equivalently the number of elements) at which the appearance seemed to change, while varying other stimulus parameters. I found that I could vary the eccentricity, size, and velocity of the envelopes by a factor of 2 in either direction, while the critical spacing required to induce a change in motion appearance remained roughly the same. Similarly I could vary the spatial frequency and temporal frequency of the carrier by a factor of 2 in either direction without much affecting the critical spacing. At the extremes of the configuration space, the change in character of the motion was present among other percepts of motion, and could become hard to distinguish. The largest effect seemed to be for spatial frequency and element size, where a change of a factor of four (going from 0.67 to 2.67 cycles per degree at 10 degrees eccentricity, the element size scaling inversely) only modestly increased the number of elements required for reversal, from 13 to 18. Scaling all spatial parameters (element size, eccentricity, envelope velocity, spatial frequency) at once did not affect the spacing at reversal; the critical spacing scaled with eccentricity.

The demonstrations shown in Figure 1 and in this section suggest that multiple motion elements placed in proximity in peripheral vision interact in such a way that the carrier motion becomes more perceptually salient and the envelope motion less so. When envelope and carrier motion are put into conflict, the inter-element spacing (scaled according to cortical distance) appears to be the most reliable determinant of which component wins. In the following sections I report psychophysical experiments designed to capture and model the determining factors explaining perceived motion direction.

3 General Methods

3.1 Observers

Observers were the author (P.B.M.) and 10 naïve observers. All had normal or corrected-to-normal vision. All observers provided informed written consent, and all procedures involved were approved by the Institutional Review Board at the University of Washington.

3.2 Equipment

Stimuli were presented on a flat CRT video monitor (ViewSonic PF790). Its resolution was set to 800×600 pixels with a display area of $35.5 \times 25.8\text{cm}$ and a refresh rate of 120Hz. Experiments were programmed in MATLAB using the Psychtoolbox (Brainard, 1997) and Eyelink toolbox extensions (Cornelissen et al., 2002), along with custom OpenGL code. All guns were fixed at the same voltage to show grayscale stimuli. The monitor was calibrated using a Tektronix J17 photometer. A gray background of $30.2\text{cd}/\text{m}^2$ was used; the black point and white point of the display measured against that background were $0.13\text{cd}/\text{m}^2$ and $60.97\text{cd}/\text{m}^2$. A hardware lookup table with 10-bit resolution was used to linearize the display response.

Observers sat behind a blackout curtain so that ambient illumination was mostly due to the monitor and viewed the screen binocularly using a chin and forehead rest with the eyes 60cm from the screen, aligned with the screen's center axis. Eye position was monitored using a video-based eye tracker (EyeLink 1000; SR Research) using a sample rate of 1000Hz. Observers gave responses by turning a knob (PowerMate; Griffin Technologies) with their preferred hand in the direction of the perceived motion.

3.3 Stimuli

This construction of the stimuli is illustrated in Figure 5. The stimuli consisted of a number of identically moving elements arranged into a circle centered on the fixation point and moving circumferentially. Each element consisted of a series of 5 motion pulses separated by a regular spatial DISPLACEMENT Δx and temporal intervals Δt . Along the direction of motion, the luminance distribution of a pulse was given by a Cauchy filter function (Klein and Levi, 1985). At right angles to the direction of motion the pulses were windowed by a Gaussian envelope with standard deviation $w/2$, while the temporal onset and offset of each pulse had a Gaussian profile with standard deviation $d/2$. An equation describing the luminance profile of a single pulse, centered at $(x, y, t) = (0, 0, 0)$ with carrier motion along x is:

$$L(x, y, t) = \cos^n(\tan^{-1}(fx/n)) \cos(\mathbf{n} \cdot \tan^{-1}(fx/n) + \omega t) e^{-(t/2d)^2 - (y/2w)^2}$$

Here ω controls the temporal frequency and f the spatial frequency of the carrier, d , the duration of the pulse, w the radial width of the envelope and n

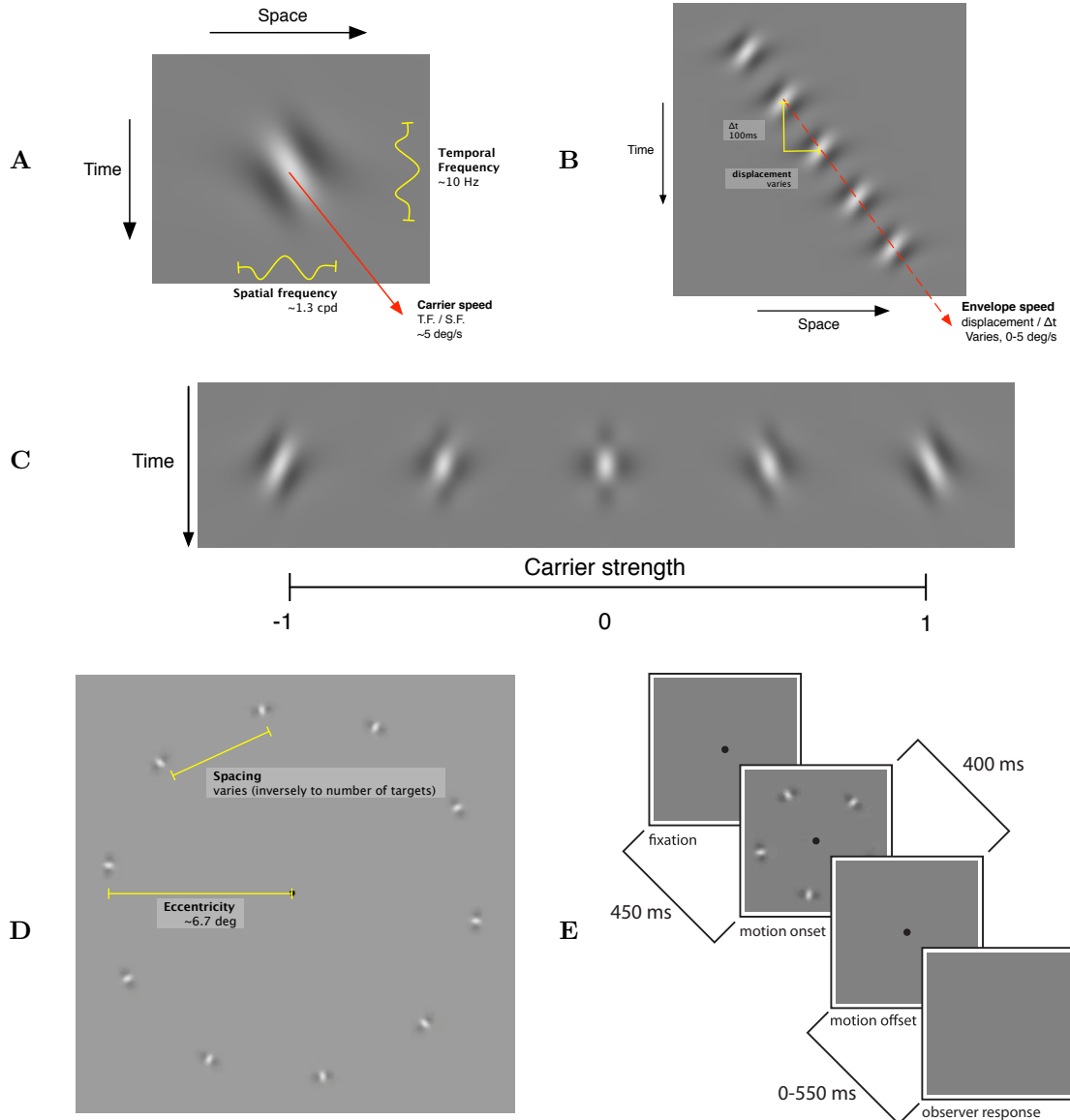


Figure 5: Construction of motion-direction stimuli. **A.** A single motion pulse, shown in a space-time diagram. Space is shown across the horizontal axis, and time is shown running down the vertical axis. Each pulse is Gabor-like with a moving carrier (visible as the local orientation in this diagram) and a fixed envelope. **B.** Motion elements were constructed of several motion pulses, offset by regular intervals in space and time. Displacement or Δx refers to the spatial displacement of the Gabor-like elements between pulses. **C.** We varied the direction of the carrier by mixing two carriers in opposite directions. A carrier strength of 0 is counterphase flicker, with equal energy along both directions of carrier motion. A carrier strength of 1 uses only the clockwise carrier. **D.** Stimuli comprised several motion elements arranged around a circle, with the directions of carrier and envelope motion along its circumference. **E.** Illustration of task. Observers fixated a central dot, viewed motion stimuli such as in Figure 6, and reported the apparent direction of motion within a prescribed time window.



Figure 6: Example stimuli. For these experiments, identically scaled stimuli were shown at 6.67 degrees eccentricity.

the circumferential width of the envelope (relative to the spatial frequency.) At the moment of maximum contrast the carrier was always in cosine phase.

To control the direction and amount of carrier motion I overlaid two pulses with opposite directions of carrier motion, with varying amounts of relative contrast. This is parameterized by the CARRIER STRENGTH C ,

$$C = \frac{C_{CW} - C_{CCW}}{C_{CW} + C_{CCW}}$$

where C_{CW} and C_{CCW} are the contrasts of clockwise and counterclockwise components. Thus C has a range of $[-1, 1]$ and a value of 0 indicates a counterphase flicker with equal parts clockwise and counterclockwise motion energy. The total luminance contrast is held at $C_{CW} + C_{CCW} = 0.5$ for the experiments reported here.

The examples in Figure 6 have the following settings, the same as used in Experiment 1 and Experiment 2: 5 pulses at intervals of $\Delta t = 100\text{ms}$, carrier temporal frequency $\omega = 10\text{Hz}$, and (with an eccentricity of $e = 6.67^\circ$,) $w = 0.5^\circ$ and $f = 2 \text{ cpd}$.

3.4 Task

The time course of a trial is illustrated in Figure 5D. A fixation point was presented. The computer then waited for the observer to fixate. 450ms after detecting fixation, the motion stimulus was shown for 400 ms (the initial pulse,

then 4 steps of envelope displacement occurring at 100ms intervals.) After the motion stimulus concluded, the observer indicated the direction of perceived motion by turning the knob within a response window from 400 to 950ms measured from stimulus onset. If the observer blinked or broke fixation before the offset of the motion stimulus, the trial was aborted and reshuffled into the stimulus set, to be repeated later in the session. If the response was outside the window, the observer received visual feedback that their response was either too fast or too slow, and the trial was also reshuffled into the stimulus set. An audio click was played each time observers gave a response; this seemed to help observers establish a consistent rhythm through the experiment. No feedback was given as to the correctness of an observer's response, only whether they had responded within the time window. Observers were instructed to report the apparent direction of motion, and advised that there were no "correct" answers. In some conditions observers reported seeing conflicting or overlapping directions of motion. In those cases they were advised to choose whichever direction of motion appeared more salient.

Observers performed the task in sessions that lasted a maximum of 1 hour, divided into 4 to 6 blocks, and were prompted to take a break between blocks. They could also rest at any time by simply delaying fixation. At the beginning of each block, the eye tracking system was automatically recalibrated by asking the observer to make saccades to a sequence of targets at randomly chosen locations on the screen.

3.5 Staircase procedure

I used staircase procedures to collect data relating the proportion of clockwise responses as to the envelope displacement, Δx . For each psychometric function we used two staircases, one 2-up-1-down and the other 2-down-1-up, to bracket the particular displacement at which subjects were equivocal about perceived direction (PSE). In a typical session, 6-8 pairs of staircases, each with a different stimulus configuration, were run concurrently, with each staircase operating independently and trials from all staircases being randomly interleaved. Example data from this procedure is shown in (figure to be placed in Results section), with envelope displacement Δx plotted on the abscissa and the proportion of "clockwise" responses on the ordinate. In these graphs we scale the area of the data points to be proportionate to the number of trials collected at that displacement. Thus, the smaller a data point, the further it may acceptably lie from the model fit; some data drawn using the smallest dots may represent a single trial at a value of displacement that the staircase procedure did not revisit.

3.6 Data folding

When staircase procedures were used, they employed randomized folding; a staircase configured to use a carrier strength C of 0.2 would actually pseudorandomly present either clockwise (0.2) or counterclockwise (-0.2) carrier on

each trial, with the staircase-controlled envelope motion reversing direction accordingly.

I similarly presume that an observer's responses to a stimulus and its mirror image are symmetric up to a constant bias. Therefore we will present and write about stimuli, without loss of generality, as though the carrier motion runs clockwise in all trials, even though the underlying data contains a balanced mixture of clockwise and counterclockwise trials. The mirror image of a trial reverses the sign of three properties: the carrier motion, the envelope motion, and the observer's response. So, a trial with carrier strength $C = -0.2$ and envelope motion $\Delta x = 0.1$, where the observer responded "clockwise," will be presented equivalently to a trial with carrier strength $C = 0.2$ and envelope motion $\Delta x = -0.1$, where the observer responded "counterclockwise." I use the convention that carrier strength is always shown as positive. Note that the direction of envelope motion can differ from that of carrier strength, so that envelope motion will still take both positive and negative values when data is folded.

In some cases observers exhibit a bias toward clockwise or counterclockwise responses. We include a global bias term in our model to account for this - this is the only term in the model that is not symmetric. We fit the model using unfolded data. When drawing fitted curves to illustrate model predictions, I sum out the bias by averaging the model predictions for clockwise and counterclockwise conditions.

4 Model details and motivation

A schematic explanation of our model is shown in [Figure 7](#). Conceptually the model combines two signals to produce decisions about motion direction: M_Δ is an estimate of the change of position of a tracked target, corresponding to envelope motion in these stimuli, and is computed within a restricted region illustrated as the smaller, black dotted circle. M_S is a sum of first order motion energy (carrier motion in these stimuli) inside a larger region illustrated by the green dashed outline. As can be seen in [Figure 1A](#), a rightward carrier on a stationary envelope may produce a perception of leftward motion. This might be accounted for by a comparison of first-order and higher order signals, so that differences between carrier and envelope are adjusted in favor of the envelope (to support motion). This is schematized in [Figure 7D](#), and appears in our model as a nonlinear repulsion term M_I appearing along with M_Δ and M_S .

For M_S , we begin by assuming that the strength of the first order motion signal is linear with respect to carrier strength C . However, as spacing decreases and there are more elements within the summation region, we expect signals from multiple elements to sum, so that the local motion signal is proportionate to the direction content of individual elements and inversely proportional to the spacing.

$$M_S = \beta_S \frac{2\pi C}{S} \quad \text{or} \quad M_s = \beta_S C N$$

Note that M_S can be expressed in terms of either element number or spacing, since the two are inversely related in Experiment 1. In Experiment 2 I attempt to disentangle these alternatives.

For M_Δ , assume that envelope motion is computed by taking the difference between successive noisy estimates of the position of a given element. The sensitivity to envelope motion β_Δ will then be inversely proportional to the uncertainty in element position. We assume that as flanking elements come closer to the tracked element, the visual system will be less able to isolate a single element to determine its position, so the sensitivity to changes in position will decline. We model this by making the sensitivity $\beta_\Delta(S)$ a sigmoid function of the spacing between elements:

$$M_\Delta = \beta_\Delta \Delta_X, \text{ where}$$

$$\beta_\Delta(S) = \beta_0 \left(2 - \frac{2}{1 + e^{-\frac{S_C}{S}}} \right) \quad \text{or} \quad \beta(N) = \beta_0 \left(2 - \frac{2}{1 + e^{-\frac{N}{N_c}}} \right)$$

This function results in sensitivity that approaches β_0 at large spacings and approaches zero at small spacings, as plotted in [Figure 7B](#). β_0 is the sensitivity to envelope displacement for isolated, uncrowded targets; S_C describes the distance over which spatial interference between targets takes place. S_C has a natural interpretation as the spacing at which the threshold for discriminating



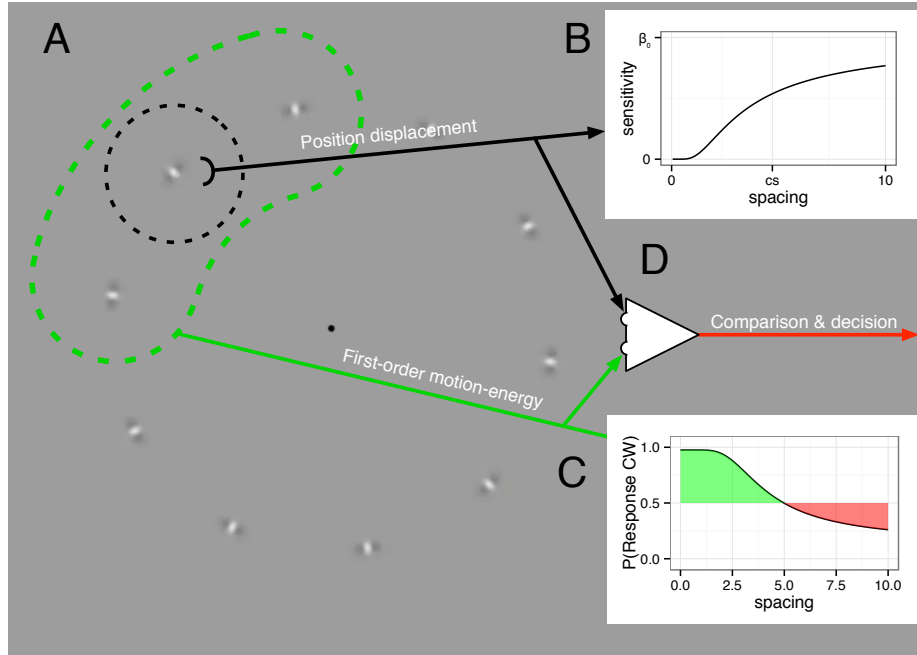


Figure 7: Schematic of motion model. **A.** The background shows a typical motion stimulus. The motion stimulus contains two sources of information. The positional displacement of an individual, attended element is computed within a limited region, as illustrated by the smaller, black dashed circle. First order motion energy is summed over a larger region, a summation of motion energy over most or all of the visual field, illustrated by the red dashed line. **B.** The higher order motion mechanism takes differences of a noisy estimate of the envelope position of a given element. Crowding interferes with estimates of position so that the sensitivity to changes in position position $\beta(S)$ is an increasing function of the flanker spacing S . We illustrate a “critical region” as the black dashed circle where interference occurs between elements. **C.** The first order mechanism sums motion energy over a large field. This mechanism is not subject to crowding; more elements in this field contribute more to the first-order motion signal. This summation region is outlined in green. **D.** The lower order and higher order signals are combined to yield a decision; there may be interactions between signals if they conflict. Thus, at wide spacings adding carrier motion to a stationary envelope may result in repulsion (shaded red region of panel C.)

a feature (in this case envelope motion) increases by a constant factor, which is often used as an empirical definition of the “critical distance” of crowding (Levi et al., 2002; Pelli and Tillman, 2008; Whitney and Levi, 2011). This function has envelope motion sensitivity reaching an asymptote for large spacing, so once elements are sufficiently far apart the number of elements does not affect sensitivity much. Again, the dependence of envelope sensitivity on envelope spacing may equivalently be expressed as a function of the number of elements, as long as elements are distributed evenly around the circle.

These two forms for M_S and M_Δ capture the phenomenon that decreasing the spacing between elements has opposite effects on the first-order and higher-order motion mechanisms. For the carrier motion signal, cramming more elements into the summation region increases the strength of the signal, since it is a simple summation of motion energy within that region. For the envelope motion signal, cramming more elements into the summation region makes it difficult to estimate the position of any individual element, and thereby weakens the signal. Thus, decreasing the spacing results in carrier motion having a stronger influence on the perceived motion, and envelope motion having a weaker influence.

One addition to this basic model is required to account for a repulsion effect I observed when carrier motion velocity disagrees with envelope velocity. In Figure 1A, it might appear to some observers that the carrier motion leftward with a stationary envelope results in perceived motion rightward, and vice versa. We account for this by a third component in the model M_I , which is a function of the average carrier strength per element. It has a linear term controlled by a coefficient β_{I_a} and a second-order, nonlinear term controlled by β_{I_b} :

$$M_I = (\beta_{I_a} C + \beta_{I_b} C|C|),$$

The nonlinear component was necessary to account for a nonmonotonic effect of carrier strength on observers’ responses (see § 5.4.5.)

These three components contribute to the modeled subjects’ responses according to a probabilistic rule:

$$\Pr(\text{clockwise} | \Delta x, C, s, n) = (1 - \lambda)\text{logit}(M_\Delta + M_S + M_I + k) + \frac{\lambda}{2}$$

where $\text{logit}(r) = (1 + e^{-r})^{-1}$ is the standard logistic cumulative distribution function. The free parameters of the model are β_0 , S_C , β_S , β_{I_a} , β_{I_b} , and k . The bias term k accounts for an overall clockwise or counterclockwise bias, which some observers exhibit. The lapse rate λ was intended to improve the robustness of the fit (Wichmann and Hill, 2001); I constrained λ to lie between 0 and 0.05.

5 Experiment 1

The movies shown in Section 2 seem to suggest that the perceived change in motion is a function not only of the properties of individual elements but of a spacing-dependent interaction between nearby elements. I explored this spatial interaction by jointly measuring the sensitivity to carrier and envelope motion as a function of the distance between elements.

5.1 Methods

Stimuli for this experiment consisted of a circle of evenly spaced elements presented at an eccentricity of 6.7° . As described above in § 3.5, I used an interleaved staircase procedure, with the staircase varying the speed of the envelope motion, and carrier strength and spacing remaining fixed for each staircase. For each session I chose a set of carrier strengths and spacings. There were two types of sessions. One type was focused on the effect of spacing, and tested several spacings at a single carrier strength, chosen based on preliminary data from that subject. Another type was focused on the effect of carrier strength, and tested a fixed set of carrier strengths (0.1, 0.2, 0.4 and 1.0), at two values of spacing. The particular values of spacing and direction content employed were selected based on preliminary sessions with that observer. There may be some adaptation when a single carrier strength or limited sets of spacings were used for an entire session. However, I found that a single model fits both datasets adequately, so data from both types of experiments are pooled and presented together here.

5.2 Results

I first show individual psychometric functions that illustrate the effects of spacing, carrier strength and envelope displacement. I found three effects relating envelope motion, carrier motion, and spacing. I will describe and show these effects qualitatively first, then show how they are accounted for by the model described in Section 4 and quantify these effects.

5.2.1 Sensitivity to envelope displacement decreases as spacing decreases

First consider the effect of changing spacing (and simultaneously increasing number) on the perception of envelope motion. There are two potential effects. A reduction in spacing may cause crowding, while an increased number of identical elements may allow summation or pooling of their identical envelope motions. These hypotheses would predict opposite effects on the sensitivity to envelope motion. Pooling would predict that more elements would lead to a greater sensitivity to envelope motion; crowding would predict that reduced spacing will reduce sensitivity to envelope motion. I found the latter; an example of this is shown in Figure 8, for a subset of the data collected. This

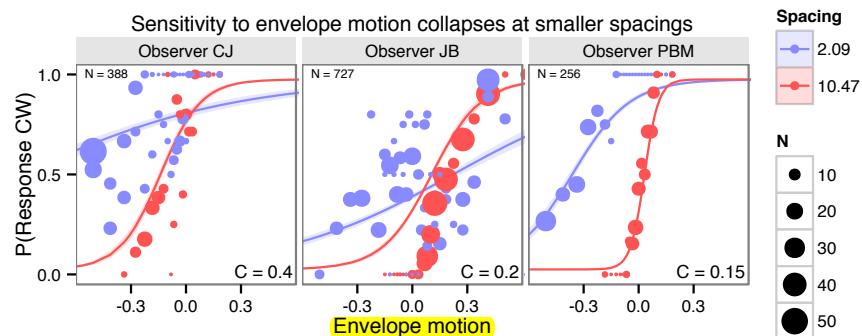


Figure 8: When spacing is reduced, sensitivity to envelope motion decreases. Data from three observers is shown, each showing two spacings. The horizontal axis shows the envelope displacement per step Δx , and the vertical axis plots the proportion of trials answering “clockwise” to that stimulus. Within each subplot the carrier strength C , written in the lower left corners, is held constant. Curves are drawn from overall fits of the model described in Section 4, using data from a larger range of spacings and carrier strengths. The points on the graph are scaled according to the number of trials made at those stimulus configurations. Therefore larger points are expected to lie closer to the model fit, while smaller points have more uncertainty and may be expected to lie farther from the model fit. In the extreme, a particular stimulus configuration might only be visited once or twice while the staircase moves past it; these smallest points would lie on either $\text{Pr}(\text{clockwise}) = 1$ or 0 . When spacings are reduced, psychometric functions fit with shallower slopes.

figure plots the envelope displacement per step, Δx , on the horizontal axis and the probability of the observer responding “clockwise” to that stimulus on the vertical axis. For Figure 8 data for two values of spacing at the same carrier strength are shown, for three observers. In each case the psychometric function fit to data collected at the smaller spacing has a shallower slope, independently of any shifts it may have. Below in § 5.4.2 I will quantify and graph the relation of sensitivity to element spacing.

Crowding causes interference at smaller distances, while pooling might still act over larger distances. Therefore I also tested whether there was a change in envelope motion sensitivity with element number at wider spacings, outside the range of spacings that might be subject to crowding, but I found no significant effect (§ 5.4.1). The values of Δx tested are substantially smaller than half the inter-element spacing, so that spatial aliasing (i.e. the wagon wheel illusion) should not explain why there is additional uncertainty in motion direction.

5.2.2 Sensitivity to carrier strength increases as spacing increases; carrier motion is repulsive at wide spacings

The responses observers made to the carrier component of the stimuli were in some ways more complicated than their responses to the envelope motion. Like was the case for envelope motion, the sensitivity to carrier motion changed as a function of spacing, but in the opposite direction (becoming more sensitive at smaller spacings.) Another feature was that carrier motion was sometimes repulsive; weak amounts of carrier motion in one direction often caused observers to shift their reports of perceived motion in the opposite direction. Thus the response to carrier motion was nonmonotonic; adding elements to a blank display caused observers to report directions of motion opposite that of the carrier, but adding more closely-spaced elements caused apparent motion to shift in the direction of carrier motion. [Figure 9](#) gives examples of both these effects, again using a subset of the data collected. This figure shows data using two different values of carrier strength, each at two different element spacings. The lower row shows data collected at the wider of the two spacings.

Of particular note in [Figure 9](#) is how observers respond when there is no envelope motion, i.e. the value of $Pr(\text{clockwise})$ when $\Delta x = 0$, where the curves intersect the vertical axis. When the carrier strength changes, a shift in this intercept reflects the sensitivity to carrier motion in the presence of stationary envelopes. The upper row in [Figure 9](#) shows data collected at small spacing, with many elements on screen, while the lower row shows data collected at smaller spacings with fewer elements. The difference between intercepts is large on the upper figure, showing that these observers are more sensitive to changes in the carrier strength when the spacing is small and there are more elements on the screen (this will be quantified in § 5.4.2.)

A second effect visible in these examples is an apparent repulsion from carrier motion at wide spacings. In the lower row, the psychometric functions fitted to this data intercept the vertical axis at values of $Pr(\text{clockwise})$ less than 0.5. That is to say, at wide spacings, observers were more likely to perceive a stimulus with stationary envelopes and clockwise carrier motion as actually moving counterclockwise. At smaller spacings, as seen in the upper row, the repulsive effect was no longer evident; when $\Delta x = 0$, observers responded clockwise, in agreement with the carrier motion rather than against it. So the repulsion may only be active at larger spacings, or it may be present at smaller spacings while being overwhelmed by a spacing-dependent effect (see § 5.4.5.)

This repulsion means that there are some stimuli for which both envelope and carrier motion are slightly clockwise, but the perceived motion is still counterclockwise; this is the case when the curves pass through the lower right quadrants in [Figure 9](#) ($\Delta x > 0$ and $Pr < 0.5$.) In these conditions the observer will respond “counterclockwise” to a stimulus whose carrier and envelope motions are both slightly clockwise. Thus at wide spacings, carrier motion repels rather than adds to the perceived direction of motion.

[Figure 9](#) illustrates that for an identical change in carrier strength, distance between the $\Delta x = 0$ intercepts for two strengths of carrier motion was much



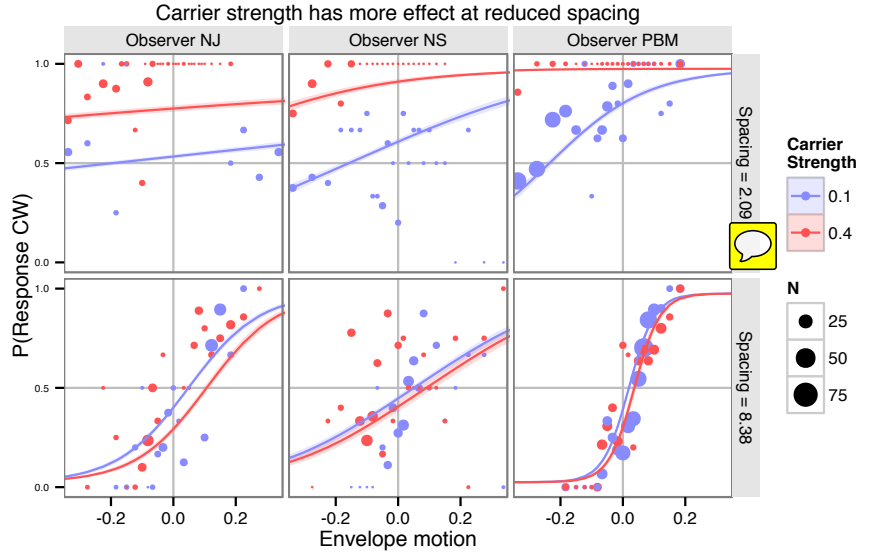


Figure 9: Reducing spacing increases the effect of carrier motion; carrier motion at large spacings is repulsive. An example subset of the data from [Experiment 1](#) is selected, showing three observers, two values of carrier strength and two spacings. The horizontal axis plots envelope displacement, the vertical axis plots proportion of responses clockwise. Colors indicate different strengths of carrier motion; three observers are shown in separate columns. Curves are predictions from a model fit to data spanning a more complete set of strengths and spacings. The upper row shows data taken using a **wide spacing**, while the lower row shows data taken at a **narrow spacing** (spacings are indicated in the right margin.) Each subplot shows two psychometric functions at two different carrier strengths. In each graph, the difference between the two curves' y -intercepts reflects the observer's sensitivity to carrier motion at that spacing. This sensitivity is greater at narrow spacings. At wider spacings, curves intercept the vertical axis below $P = 0.5$, indicating a tendency to respond in opposition to the carrier motion.



larger at the narrow spacing than at the larger spacing. (This will be quantified in § 5.4.2.) Note that this statement about sensitivity is based on the shift in the vertical axis intercept, rather than the shift in the point of subjective equality (the intercept with the horizontal line $P = 0.5$.) One would expect the distance between the points of subjective equality to be increased even if the strength of carrier motion did not change, because of the change in slopes: an identical vertical shift applied to two lines will produce a greater shift in the x-intercept for the line with the shallower slope. However, since the change in vertical axis intercept is also larger at smaller spacings, it appears that the sensitivity to carrier motion has increased in addition to the decrease in sensitivity to envelope motion.

Figure 9 presents folded data, i.e., values shown here with a single value for carrier strength, which I nonetheless refer to as “clockwise,” represent data collected from both that stimulus and its mirror image, and envelope motions and responses are mirrored correspondingly. So a point appearing below $P < 0.5$ in this graph can be read as indicating that the observer chose “counterclockwise” to a particular stimulus more often than they chose “counterclockwise” to that stimulus’s mirror image. Thus the presentation of folded data here averages out any static biases toward one direction.

In the previous section I illustrated that the sensitivity to envelope motion, visible as the slope of the psychometric function, decreased when element spacing decreased. In this section I illustrated that carrier motion has the opposite change in sensitivity; carrier motion has a stronger influence on perceived motion for narrowly spaced stimuli. In this experiment the spacing between elements covaries with the number of elements, so that it is indeterminate whether either effect should be considered an effect of the reduced spacing or of the increased number. However, in either case, this contrast identifies a way in which higher-order motion is processed differently from first-order motion; it appears that envelope motion signals from separate objects cannot be combined in this task, while carrier motion does appear to combine between adjacent objects.

5.3 Model and data visualizations

Having given examples illustrating some of the effects that a model should capture, this section attempts to present an overview both of the entire dataset, and how the model specified in Section 4 fits that data. In the subsequent section I will examine particular features of the model and evaluate their fit to the data.

This experiment related three parameters – carrier strength, envelope motion and spacing – to a fourth variable, the motion perceived by the observer. One can visualize those variables as forming a three-dimensional space illustrated in Figure 10. The combination of these three variables determines the likelihood with which the observer will respond “clockwise” or “counterclockwise” to the given stimulus. The model’s prediction of the proportion of responses clockwise visualized as a density coloring each point in the space. Four planar sections are shown through this space to highlight model features of interest. In Figure 11

these same planar sections are pulled out and shown in relation to the observed data.

5.3.1 Model figure construction

[Figure 10](#) and [Figure 11](#) show data from one observer; the complete set of illustrations for all observers is shown in an appendix. The background color scale depicts the probability of responding “clockwise”, with high probabilities shaded red and low probabilities (i.e. tending counterclockwise) shaded blue; probabilities further from 0.5 in either direction are shown with darker and more saturated colors. The four subplots correspond to the four planes shown in figure [Figure 10](#).

Each panel in [Figure 11](#) shows the model’s predictions as a function of two of the three variables, leaving the other fixed; the value of the fixed variable is noted in the upper right corner of each panel. The four panels show how model responses vary (UPPER LEFT) as a function of spacing and carrier strength, for stimuli with zero envelope motion, (LOWER LEFT) as a function of spacing and envelope movement, for stimuli with zero carrier strength, (UPPER RIGHT) as a function of envelope motion and carrier strength, for stimuli with a fixed, wide spacing, and (LOWER RIGHT) as a function of envelope motion and carrier strength (same slice direction as UPPER RIGHT), for stimuli with a fixed, narrow spacing.

[Figure 11](#) also represents the observer’s responses. Trials are sorted into bins according to stimulus parameters and a summary circle is plotted for each bin. The circles are drawn with area proportional to the number of trials they summarize. The shade within the circle is a weighted average of the observer’s responses. Any difference between the shading inside the circle and that of the background indicates a residual between the model and the subset of observed data summarized in that circle. Each plot uses a different binning, according to its axes. For example, a circle in the lower left figure summarizes a set of trials with a particular range of envelope motion and spacing, but any value of carrier strength.

5.3.2 Binning and color scaling

This section gives technical details of how responses are binned and averaged for display in [Figure 11](#). The shading within each circle is not simply the arithmetic mean of observers’ responses, but is based on the difference between the data and model predictions. I based the plot on the residuals rather than the sample mean for reasons related to the three dimensional parameter space and the sampling of data throughout that space. First, each circle represents the subset of trials that lie closest to it in the two dimensions of the plot, but these trials may be located at any value in the third dimension. For example, in the UPPER LEFT panel, showing a slice across carrier strength and spacing, data are combined across all speeds of envelope motion. The response probability varies in the unseen dimension, so that one circle may combine stimuli for which the observer

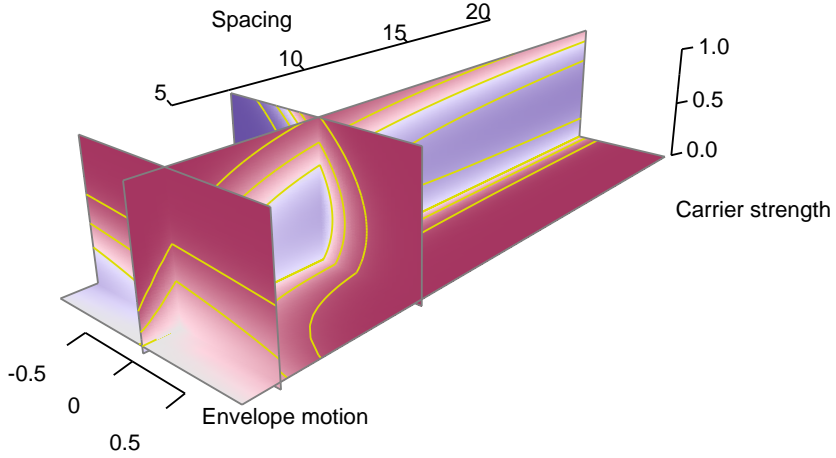


Figure 10: A three-dimensional representation of the model fit for one observer (NJ). Axes correspond to the three stimulus parameters varied in this experiment: inter-element spacing S in degrees, envelope motion Δx , in degrees per step, and carrier strength C . The background color scale indicates the probability of responding clockwise predicted by our model. Four planar sections through the three-dimensional space are shown, and correspond to the four panels in figure Figure 11. Red shades indicate stimuli for which the model predicts responses that agree with the direction of carrier motion (whose strength is plotted on the vertical axis) and blue shades indicate stimuli where the model's predicts responses that disagree with the direction of carrier motion. In both cases the luminance depends the difference between the response probability and 0.5, with response probabilities further from 0.5 are colored darker and more saturated. Yellow contour lines are placed at response probabilities of 0.1, 0.3, 0.5, 0.7 and 0.9.

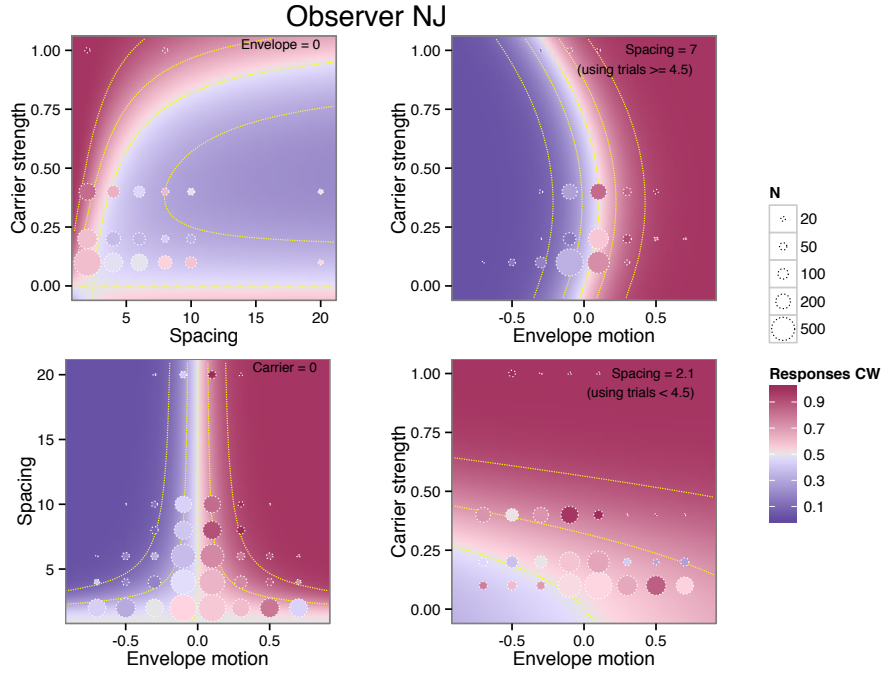


Figure 11: Data and model responses for observer NJ. The four plots shown correspond to the four planes shown in Figure 10; color scale and contour line placement are the same. Circles represent observers' recorded responses for trials whose parameter are binned near that stimulus. The shading of each circle depends on the residual between the recorded responses and the model prediction for that set of stimuli; an identical shade inside the circle as outside indicates no residual, and the shading should be interpretable on the same scale as the probability scale of the background. Each circle summarizes the subset of trials falling near that point in the two dimensions of its panel. UPPER LEFT: Response probability as a function of spacing and carrier strength, with envelope motion fixed to zero. Residuals collect trials across all envelope motions (see § 5.3.2.) LOWER LEFT: Response probability as a function of envelope motion and spacing, for stimuli with no carrier strength (i.e. counterphase flicker). Residuals collect trials across all carrier strengths. UPPER RIGHT and LOWER RIGHT: Fitted model response as a function of carrier spacing and strength, for two different values of spacing (indicated in the upper right). Residuals shown in the upper right are of trials with spacing from 4.7 to 21 degrees, while residuals shown in the lower right are of trials with spacing between 1.7 and 4.2 degrees.

tends to respond clockwise with stimuli for which the observer tends to respond counterclockwise. Indeed since I used a staircase procedure to choose envelope displacement, the the mean response probability in each bin clusters around 0.5, which would not be useful to display. Since the data are not uniformly sampled throughout the stimulus configuration space, adjacent bins collect trials with a different sampling in the unseen dimension, as determined by the staircase procedure. A simple arithmetic mean of each bin would not lead to a depiction of observed data that could be visually compared with either adjacent bins or the model on the 2-d slice.

Instead the shading within each circle is determined by computing the Pearson residual between model predictions and observations, then applying that residual at the location of the bin center to obtain a remapped response probability. Consider n trials, whose parameters are x_i and responses are y_i , falling within a bin centered on a certain stimulus configuration \bar{x} . Recall that the Pearson residual for a set of n binary observations y_i and corresponding model predictions $\hat{\mu}_i$ is defined as

$$R = \frac{\sum_i (y_i - \hat{\mu}_i)}{\sqrt{\sum_i \hat{\mu}_i \cdot \sum_i (1 - \hat{\mu}_i)}}$$

which is the total difference between data and observation scaled by the expected standard error. If the model $\hat{\mu}$ is a function of the stimulus parameters x so that $\hat{\mu}_i = \hat{\mu}(x_i)$, I define a remapped response probability $\bar{y}(x)$ in terms of the Pearson residual,

$$\bar{y}(x) = \hat{\mu}(x) + R \frac{1}{\sqrt{n}} \sqrt{\hat{\mu}(x)(1 - \hat{\mu}(x))}$$

The shading of the circles in Figure 11 is chosen according to $\bar{y}(x)$, while the background is colored according to $\hat{\mu}(x)$. This is designed so that the difference between background and observation drawn on the graph fairly depicts the difference between model fit and data: if the Pearson residual is zero for a bin of trials, then $\bar{y}(x) = \hat{\mu}(x)$; if all the parameters happen to fall at the bin center so that all $x_i = x$, \bar{y} collapses to the sample mean $\bar{y}(x) = \frac{1}{n} \sum_i y_i$, and for a given set of random observations y_i , $\bar{y}(x) - \hat{\mu}(x)$ is proportional to R .

Figure 11 does not include a measure of standard error or significance because all dimensions in the figure are already mapped to stimulus variables. Below in § 5.4 will consider model predictions and data one variable at a time, at which point I can display standard errors of observed and predicted data and obtain goodness of fit statistics. However, the areas of the plotted circles in Figure 11 are scaled to the number of observations, which may help give a sense of the significance of differences between model and data; one expects larger circles to have less difference between observation and model.

5.3.3 Phenomena captured in the model

The four plots in Figure 11 illustrate effects associated with carrier strength, envelope motion, and spacing. The lower left panel shows how the observer's



response varies for stimuli with no carrier motion (i.e. with all elements flickering in counterphase.) The horizontal axis measures the degree of carrier motion used in the stimulus, while the vertical axis measures the inter-element spacing. When there is no carrier motion, observers tend to report clockwise apparent motion for envelope motions that are clockwise, and vice versa. This is reflected by the right half of the graph taking values greater than 0.5 (in red) and the left half of the graph taking values less than 0.5 (in blue.)

The effect captured in the lower left panel is how the sensitivity to envelope displacement (which corresponds to the inverse of the horizontal distance between contour lines) changes as a function of spacing. In the model the spacing-dependent sensitivity is described by the function $M_\Delta(S)$ and is controlled by the sensitivity parameter β_0 and the “critical spacing” parameter S_C . The sensitivity to envelope motion decreases at smaller spacing, causing contour lines to spread apart at the bottom of the graph. The data that is observed, whose residuals are plotted in circles, shows analogous behavior. Note that at smaller spacings, data has been collected over a wider range of envelope speeds than at the larger spacings. This is a result of using a staircase procedure which steps over a wider range when the sensitivity is lower. Even at the smallest spacings most data has been collected with envelope step sizes significantly smaller than half the spacing, so that the ambiguity of forming correspondences between element appearances (i.e. the wagon wheel illusion) should not contribute to the lessening of sensitivity.

The upper right panel of [Figure 11](#) characterizes responses to envelope and carrier motion at a wide spacing. Consider starting at the point $(0,0)$, where the response probability is 0.5. Traveling up the graph, corresponds to adding carrier motion to the stimulus; response probabilities at first drop below 0.5, exhibiting repulsion. Increasing the carrier motion further, the repulsion reverses and the observer now reports motion in the direction of the carrier. At any point, moving horizontally corresponds to a change in the envelope motion; at the large spacing captured in this graph, sensitivity to envelope motion is high.

The lower right panel has the same axes as the upper right but shows narrow spacings. Moving vertically in this graph gives a large change in response, reflecting a higher sensitivity to carrier motion than in the upper right panel. By comparison, moving horizontally shows much less sensitivity to envelope motion than in the upper right panel. The repulsion effect M_I that was evident in the upper graph is swamped by the higher sensitivity to carrier motion M_S .

Finally, the upper left panel shows the combined effects of both the nonlinear repulsion and spacing-dependent summation effects. Here the envelope motion is fixed to zero. At relatively wide spacings, moderate carrier strengths induce repulsion, indicated by mostly blue colors on the right side of the panel. Carrier strengths less than 0.4 generally cause repulsion but as the carrier strength approaches 1 again, carrier motion once again becomes positive in strength. The repulsion effect also disappears at narrower spacings. Both the repulsion at weak carrier strengths and its reversal at at high carrier strengths occurred for most observers in the dataset.

The repulsion effect M_I is modeled as a function only of the carrier strength;

it is independent of both the number of elements on the display and the spacing between them. I explored changing or adding similarly formulated terms that were dependent on element number and on spacing, but these did not result in better fits as assessed by the AIC measure (Akaike, 1974).

While sensitivity to envelope motion decreases when spacing is reduced, the sensitivity to carrier motion typically increases. The combination of the two effects can be seen in comparing the upper right and lower right panels of Figure 11. When spacing is relatively wide, as in the upper right panel, the gradient of the decision function is steeper along the axis of envelope motion, and the model is relatively insensitive to carrier strength. In the lower left graph, showing data at narrow spacings, the situation has reversed. Broadly speaking it appears that motion is driven by envelope motion at wider spacings but by the carrier motion when spacing is narrow.

Similar patterns of behavior are found for most observers. The set of plots for all observers who participated in this experiment is included in Section 10.

It is worth noting the areas where the model is not fully successful at reproducing observers' data. Often the repulsion measured at a carrier strength of 0.2 is stronger than the model fit, and the repulsion at 0.4 is weaker (see Figure 14 below.) This suggests that the functional form I have chosen for $M_I(C)$ might need to be improved, however the current data do not have the power that would select a better principled parameterization.

Another area where the model does not fully capture the observers' behavior is that their responses at smaller spacing are more variable than the model would predict. This is visible to some extent in the raw data plotted in Figure 8; the data collected at wider spacings trace out a psychometric function, but the data collected at narrower spacings have more dispersion than one would expect from the model fit. This is also visible in the bottom row of circles in the lower left panel of Figure 11, where the differences between model and observed data are more apparent.

5.4 Model components, effect sizes, and goodness of fit

This model captures the effect of three factors - carrier strength, envelope motion and spacing - that each affect perceived motion. This model also captures variation in the appearance of these stimuli between observers, since changes in model parameters can lead to different predicted perceptions of the same stimuli. In the following sections I attempt to check the model's performance in describing behavior with reference to its three components. This will help evaluate and provide some justification for the particular functional forms that have chosen in our model, as well as show how each effect is consistent across observers, while their proportions vary.

Tests of goodness of fit such as residual deviance and Pearson χ^2 operate by comparing the predictions to those of a saturated model, one with as many parameters as observations that captures all the variance. However the idea of a saturated model does not have a perfect equivalent in the case of binary responses, and analogous fit tests are problematic when the predictors are not

evenly grouped (Collett, 2003), or when the observations sparsely sample the space spanned by multiple predictors (Hosmer et al., 2013), both being situations which characterize this dataset.

Further, applying an complete goodness of fit test to a model with multiple effects involving multiple predictors would not give a useful evaluation of how well each component effect is capturing behavior. Therefore it would be most instructive to focus on the fit for each effect considered separately. Since I sampled a discrete set of spacings and of carrier strength, this can be done by expanding the proposed model m_P into model $m_{S,E}$ that is saturated over one predictor E ; i.e. adding indicator variables for each value of spacing or carrier strength, and fitting the sensitivity in terms of those indicators. This builds a “effect saturated” model $m_{S,E}$; a corresponding process builds a null or intercept model $m_{0,E}$. Then the success of each effect term can be characterized by nested comparisons between null, proposed (m_L) and saturated models (Tsiatis, 1980; Archer et al., 2007), and by the log-likelihood-based pseudo- R^2 measure

$$R_{L,E}^2 = \frac{L(m_P) - L(m_{0,E})}{L(m_P) - L(m_{S,E})}.$$

Perhaps more importantly, building effect-saturated models allows visual comparison of, e.g., how the sensitivity to carrier motion varies over each discrete value of spacing tested, versus the model’s behavior over the same question.

5.4.1 Lack of pooling of envelope motion across large distances

I motivated the description of the model proposed in Section 4 by considering that the observer attends a single element of the display; other elements are not attended, may but exert an influence via crowding or summation. However, in our task the stimulus is composed of identical, identically moving elements. Therefore in principle, it is not necessary that an observer isolate any particular element to measure envelope motion; any element or combination of elements will do the job. When distinct objects move concurrently, one can perceive the motion as being of a larger element of which the distinct components are features, such as in Ternus displays (Boi et al., 2009) or as being components of a larger rigid body (Anstis and Kim, 2011). In the present stimuli, both envelope and carrier motion are, considered separately, consistent with that of a wheel rotating around the fixation point. Knowing this, an observer might pool multiple envelope position signals in order to improve sensitivity to envelope motion. If that is the case than the sensitivity to envelope motion (i.e. the slope of the psychometric function relating envelope motion to response probability) should increase when additional, coherently-moving elements are added to the display, as long as targets remain widely separated enough to avoid crowding.

For 9 of the observers who participated in this experiment, I collected data with both 2 and 4 elements on the display (at an eccentricity of 6.67°, corresponding to spacings of 20.9° and 10.5° around the circle.) These spacings should be large enough to escape crowding effects. To assess the presence or absence of pooling at large distances I compared observers’ sensitivities to envelope

displacement at 2 and 4 elements using a logistic regression model formulated as

$$\Pr(\text{clockwise} \mid \Delta x, C, n) = \text{logit}(\beta_n \Delta x + k_{|C|,n} C + b_{|C|,n})$$

where the slope of the psychometric function corresponds to β_n and separate proportionality constants k and b were used for each absolute value of direction content and element number. Using a treatment contrast for β_n , I asked how sensitivities changed as a function of element number. For 6 of the observers, the sensitivity coefficient decreased at 4 elements as compared to 2; for the remaining 3 it increased. However, any change only reached a significance level of $p < 0.05$ for only one observer (whose sensitivity decreased as element number changed from 2 to 4.) The subset of data considered here comprises 5561 trials. I conclude that there is not pooling of envelope motion data between separate objects in this experiment, which agrees with the choice of a form of $\beta_\Delta(S)$ which reaches an asymptote at large spacings.

5.4.2 With shorter distances between elements, sensitivity to envelope motion declines.

A central feature of the proposed model as illustrated in Figure 7 is that it expects the sensitivity to envelope motion to decline as spacing between elements declines, i.e. there is a crowding effect on the detection of envelope motion. As described above, to assess whether the model captures the effect of spacing on sensitivity in the presence of other effects, I compare the proposed model to a null model without this effect and a saturated model formed by expanding the parameterization of $\beta_\Delta(S)$ into a set of dummy variables coded to capture a different value $\beta_{\Delta,S}$ for each distinct value of spacing tested. The null model uses a constant value of sensitivity at all spacings. All other aspects of the model are left as described in Section 4.

The proposed and saturated models are plotted in Figure 12 for three observers (the entire set is shown in Figure 47.) The measurement obtained in the saturated model is noisy, but the sensitivities do approach zero as spacing approaches zero. Also confirming the analysis in § 5.4.1, as spacings become large, sensitivity appears to reach an asymptote. So both general features chosen for the functional form of $\beta_\Delta(S)$, an asymptote at large spacings, and a collapse to zero at small spacings, are consistent with the data. Comparing the proposed to the null model, all observers show highly significant improvements, with the largest p -value being 10^{-5} . Further comparing the proposed to the saturated model, 3 out of 11 observers show a significant difference between proposed and saturated model.

Labels in each facet of the plot show the pseudo- R_L^2 measure described above. Aggregating across all observers, I obtain a value of $R_L^2 = 0.58$. Note that for observer PBM (the author) the sensitivities are much larger than for other observers, while still showing the same form of collapse at narrow spacings. The higher sensitivity might be attributed to overtraining relative to the naïve observers.

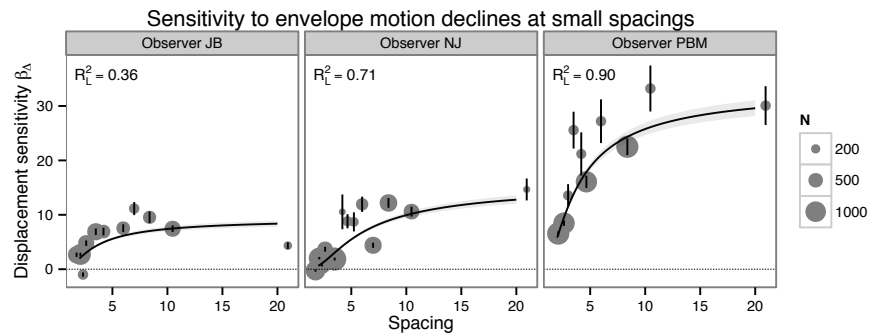


Figure 12: Sensitivity to displacement collapses as spacing decreases. In each subplot, the horizontal axis denotes spacing, while the vertical axis measures sensitivity to direction content (corresponding to the slopes of the psychometric functions shown in Figure 8.) Data points are obtained by re-fitting the model while allowing sensitivity to vary freely for each value of spacing, while other aspects of the model are unmodified. Vertical segments at each point indicate \pm standard error and the size of each point indicates the number of underlying trials. The vertical axis is the sensitivity to envelope motion (corresponding to the change in log-likelihood of answering “clockwise” to a stimulus when changing Δx by 1° .) Curves show the prediction of our model fitted to the same data $\beta_{\Delta x}(S)$, as a function of spacing S . Three observers are shown here; the complete set is shown in Figure 47.

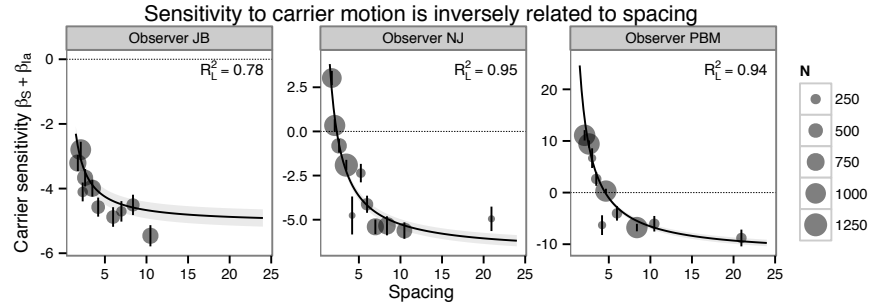


Figure 13: The sensitivity to carrier direction content increases at smaller spacings. The vertical axis measures the sensitivity to carrier motion $M_s(S)$ as a function of spacing. Individually plotted points are obtained by letting this coefficient vary freely for each value of spacing; curves indicate model predictions. Vertical segments at each point indicate \pm standard error and the size of each point indicates the number of underlying trials. Because the sensitivity and amount of repulsion vary between observers, each panel has a different scale on the vertical axis; the dotted horizontal line indicates a sensitivity of 0, which marks the boundary between assimilation and repulsion for small amounts of carrier strength. Data from three observers are shown here; the complete set is shown in Figure 48.

5.4.3 At shorter distances, carrier motion summates, causing an increase in sensitivity to carrier direction content.

While the sensitivity to envelope motion decreases as flanking elements are brought closer, the sensitivity to carrier motion increases ~~at the same time~~. I assessed this effect using the same technique as before, forming a saturated model by dropping the term $M_s(S)$ and including variables $\beta_S C$ for each distinct value of spacing. The saturated model also covers the linear repulsion term $\beta_{I_a} C$ (as it is proportional to carrier strength and thus linearly dependent with the dummy variables.) The other components of the model remain, including the nonlinear component of repulsion $\beta_{I_b} C |C|$. The null model retains the term $\beta_{I_a} C$ (i.e. it has a constant sensitivity to carrier motion that does not vary with spacing.) For data at a few spacings tested at a carrier strength of 1, responses align completely with carrier motion direction, which leads to undefined likelihoods for those data in the saturated model; those data are disregarded for purposes of model comparison.

The comparison of proposed and saturated models is shown in Figure 13. The units β_S are interpretable as the change in log-odds of responding “clock-

wise” in proportion to a small change in the carrier strength. For several observers the inverse proportion to spacing captures the response very well. Likelihood ratio tests show significant improvements from null to proposed models for all of observers; in aggregate, the proposed model is successful, obtaining $R_L^2 = 0.7874$ with reference to null and saturated models. The functional form relating carrier sensitivity to the inverse of spacing appears to be a good fit, obtaining $R_L^2 = 0.7874$ over 0.9 for 3 observers. However, some observers are not as well fit (Figure 48.) Note that for some observers such as JB the measurement in the previous section does not find assimilation even at the smallest spacings, however the sensitivity measure here is a discounts the nonlinear repulsion term $\beta_{I_0} C |C|$ which can turn increments of carrier motion assimilative at higher carrier strengths.

5.4.4 At larger spacing, weak carrier direction content repels direction judgments.

Note that carrier sensitivity measured in the previous section, in addition to the inverse proportionality to spacing, has a constant generally negative offset. I have referred to this offset as “repulsion,” since negative values of carrier sensitivity means that increments in carrier strength bias the observer’s judgements in the opposite direction. Thus, in Figure 13 carrier sensitivity does not approach zero at large spacings, but some usually negative value. Carrier motion generally become assimilative when there are more, closely packed elements in the display. The first is that the strength of repulsion seems to be determined by the carrier strength of an individual element, rather a sum over nearby elements. That is, after accounting for summation, which as we saw in § 5.4.3 can be well fit by a term proportional to the number of elements, there is a remainder that appears to be independent of the number of elements or their spacings. This repulsion effect is independent of element spacing, while the spacing-dependent component of carrier strength is directly proportional to the number of elements; this might indicate some element of carrier motion processing that is independent of the number of elements or their spacing.

5.4.5 The repulsion effect is nonlinear in carrier strength.

At carrier strengths approaching 1, the repulsion effect can weaken and even reverse. This effect is visible in the upper left panel of Figure 11, where moderate values of carrier strength at wider spacings are repulsive (blue shades) but become assimilative (red shades) as carrier strength is further increased. The spacing-dependent assimilation effect contributes to this, but is not strong enough at wide spacings to account for the reversal of perceived motion. There are two notable characteristics of this repulsion. The first is that the degree of repulsion appears to be a nonlinear function of direction content. This repulsion is captured in the model in the function $M_I(C)$. This can be understood as a component of the observer’s response that is a function of the carrier strength but is independent of the element spacing or number.

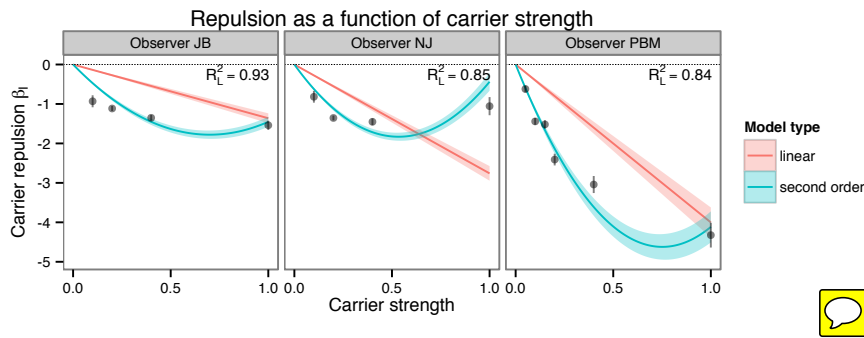


Figure 14: Effects of motion repulsion at wide spacing. The vertical axis shows the response rate to stimuli with zero envelope motion at a nominal spacing of 10° with the horizontal axis showing the carrier motion. Data points are obtained from a model whose repulsion term is saturated over carrier motion (see § 5.4.) Curves illustrate predictions from two alternative models, one where repulsion is a linear function of carrier strength, and another where there is a second-order nonlinearity. The second order model obtains a better fit (see section § 5.4.5.) R^2_L values are computed with reference to a null model which has no repulsion. Under this model, all but one observer (the complete set is plotted in shows a negative slope of the curve where direction content crosses zero, indicating a repulsive effect for weak carrier strength, while the second order coefficient weakens or reverses this effect for stronger carriers.

Similarly to previous sections, I analyze the presence of this nonlinearity by comparing nested models. The null model has no effect of carrier motion, i.e. $M_I = 0$, but is otherwise identical to the full model described above in [Section 4](#). The second model is one in which the repulsion is linearly related to the carrier strength of the stimulus; $M_I = \beta_I C$. For the linear model, 10 out of 11 observers showed a significant ($p < 0.05$) improvement over the null model. However, the linear model does not capture the observation that while weak carrier strengths repel motion direction judgements, stronger carrier strengths do not. The proposed model adds a second-order, odd-symmetric component to repulsion signal; $M_I = \beta_{I_a} C + \beta_{I_b} C |C|$. As compared to the linear model, I found that for all 11 observers, the fit was significantly improved by adding the second-order component, the largest p -value being $p = 2.4 \times 10^{-7}$ for observer CJ.

Additionally, while the signs of β_I in the linear model are mixed, the second-order model is more consistent between observers. Every observer with the exception of CJ has a negative value of β_{I_a} and a positive value of β_{I_b} , indicating that small imbalances of motion energy at wide target spacings usually lead to repulsion, but that the repulsion is proportionately weaker, or even reverses, with stronger direction content.

[Figure 14](#) plots the the strength of repulsion as a function of carrier strength. The figure shows fitted curves for the linear and second-order models, and data points corresponding to a saturated model. As mentioned above, for all observers except CJ, the slope of the linear component of the second order model is negative, indicating a repulsive effect of carrier motion; for the same observers the coefficient of the second-order component is positive, indicating that the repulsion proportionately weakens, or in some cases reverses, when direction content approaches $|C| = 1.0$. The computed values do not include the spacing-dependent summation effect, which is also proportional to carrier strength; when both effects are added together the model obtains the behavior of repulsion at moderate carrier strength but summation at high carrier strength that are observed in the data. Aggregated over all observers, the second order model obtains a score of $R_L^2 = .66$ with reference to a saturated model.

10 Model fits and data for all observers

In this section I show the complete collection of model and diagnostic plots for all observers.

10.1 Model fits in perspective and contour plots

The following figures illustrate the main effects of the motion model described in [Model details and motivation](#) as fitted to each observer's data. They are formatted identically to those presented earlier in [Experiment 1](#) and [Model and data visualizations](#).



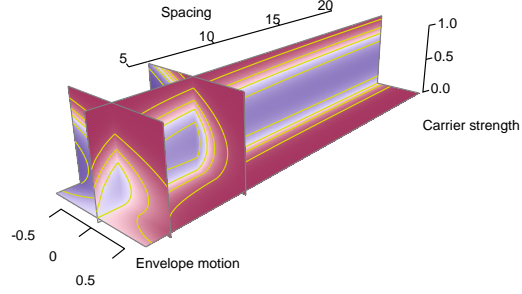


Figure 25: Perspective view of fitted model for observer AS. The format of the plot is the same as figure Figure 10.

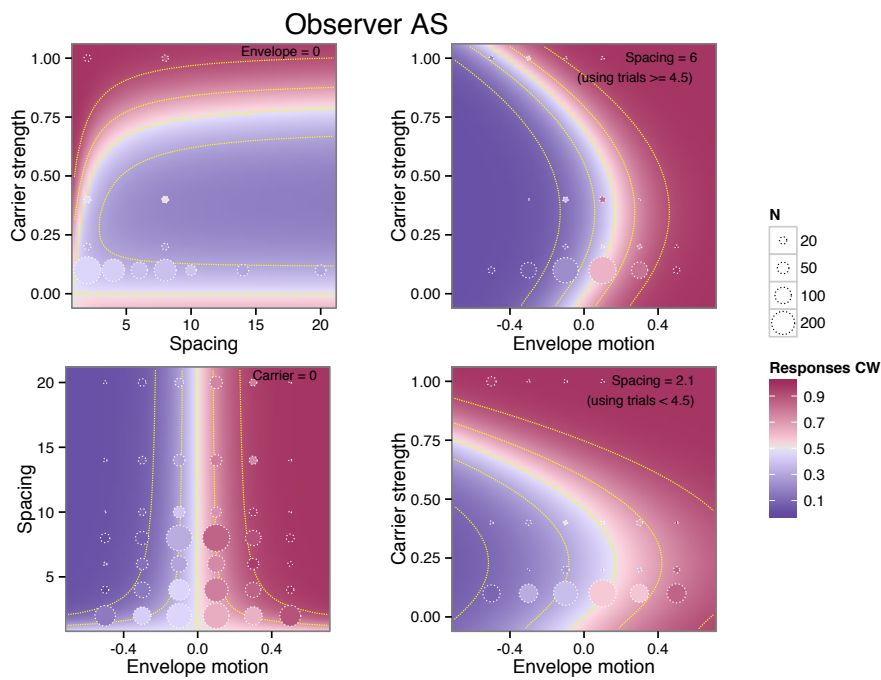


Figure 26: Model fits and summary of data for observer AS. The format of the plot is the same as figure Figure 11.

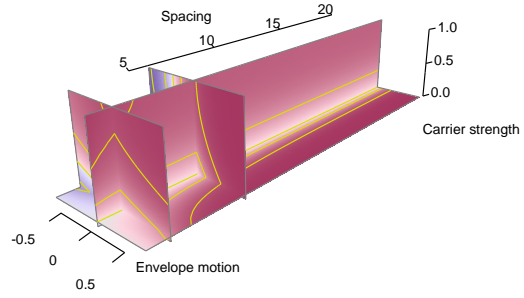


Figure 27: Perspective view of fitted model for observer CJ. The format of the plot is the same as figure Figure 10.

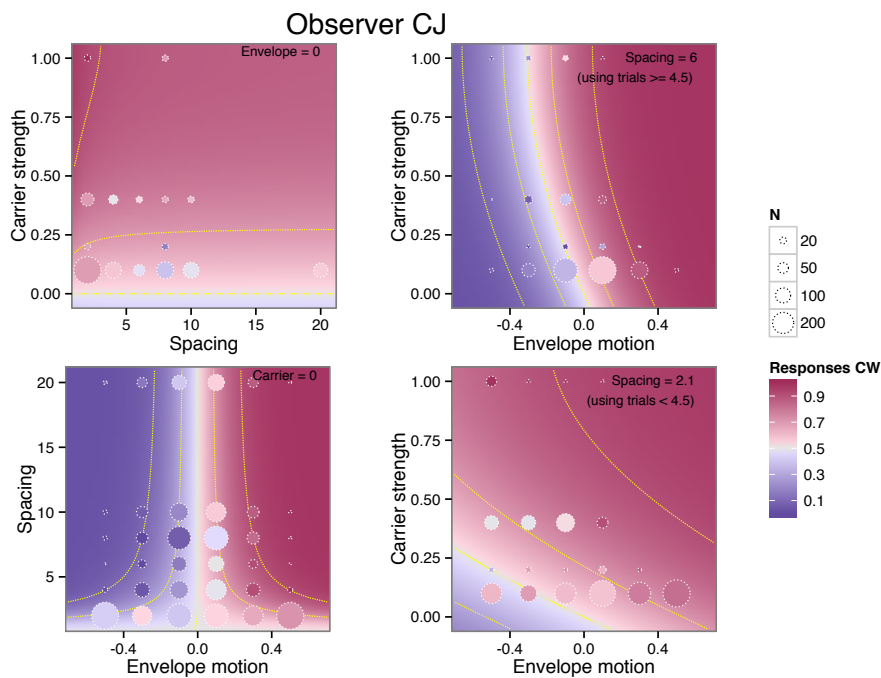


Figure 28: Model fits and summary of data for observer CJ. The format of the plot is the same as figure Figure 11.

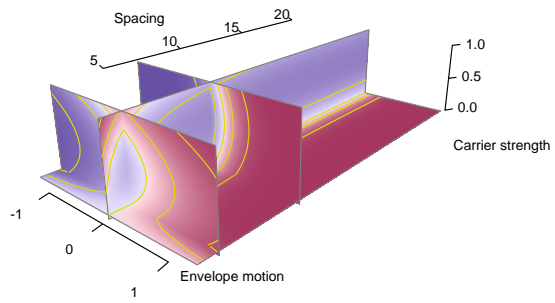


Figure 29: Perspective view of fitted model for observer JB. The format of the plot is the same as figure Figure 10.

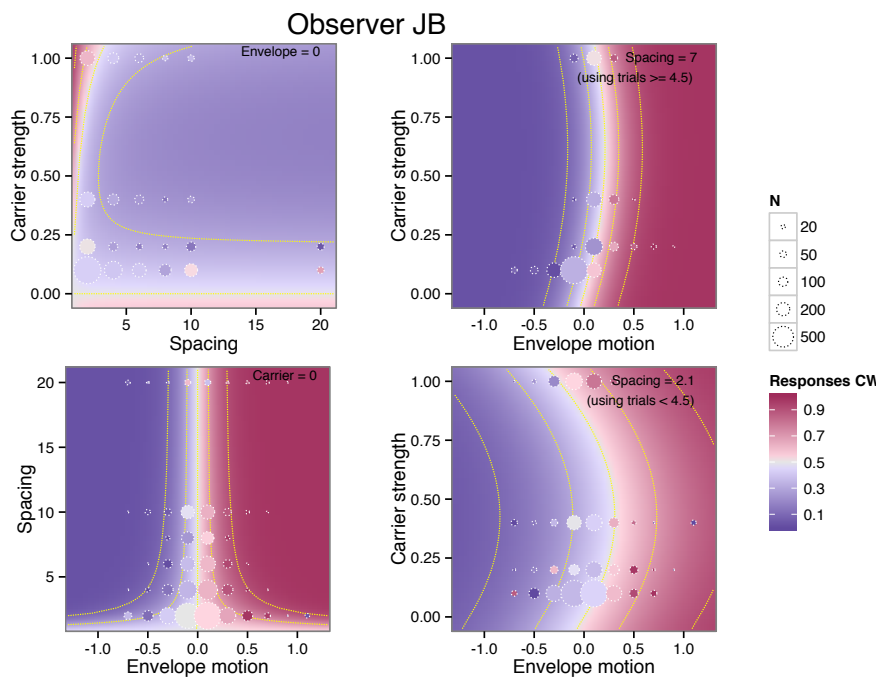


Figure 30: Model fits and summary of data for observer JB. The format of the plot is the same as figure Figure 11.

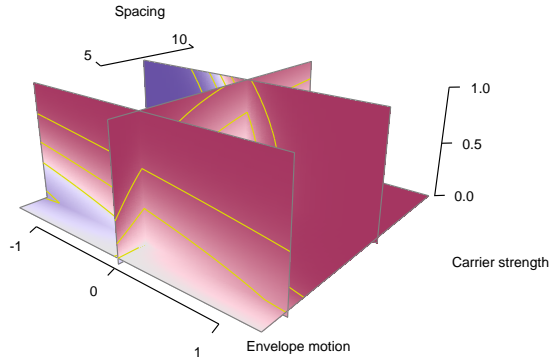


Figure 31: Perspective view of fitted model for observer JE. The format of the plot is the same as figure Figure 10.

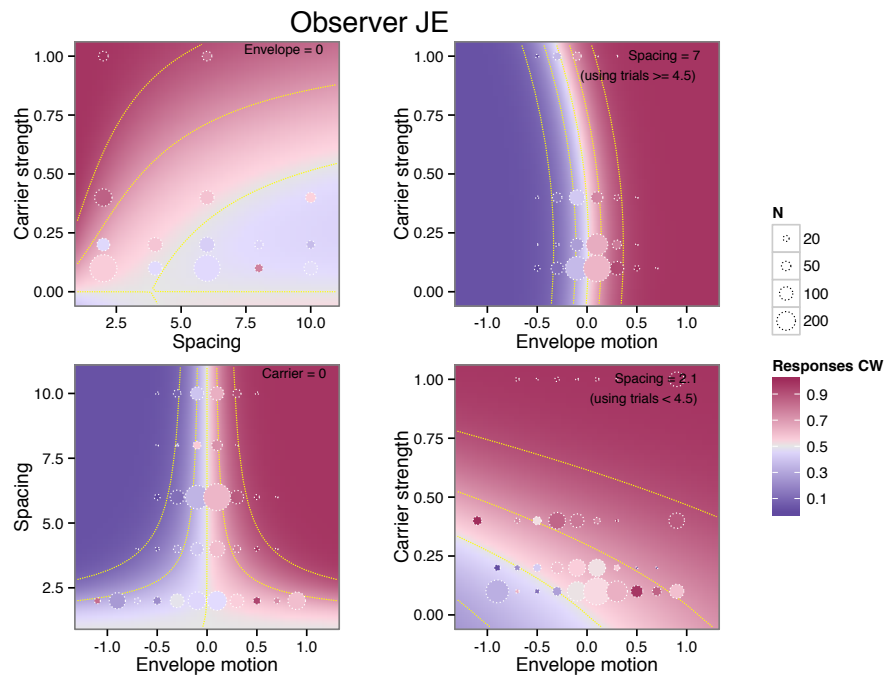


Figure 32: Model fits and summary of data for observer JE. The format of the plot is the same as figure Figure 11.

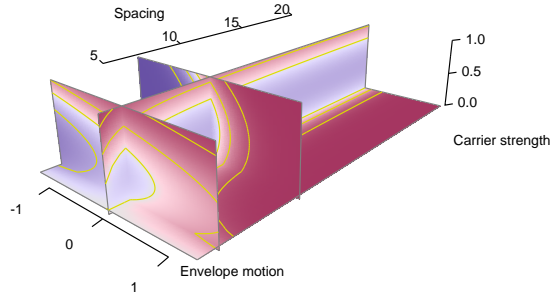


Figure 33: Perspective view of fitted model for observer KO. The format of the plot is the same as figure Figure 10.

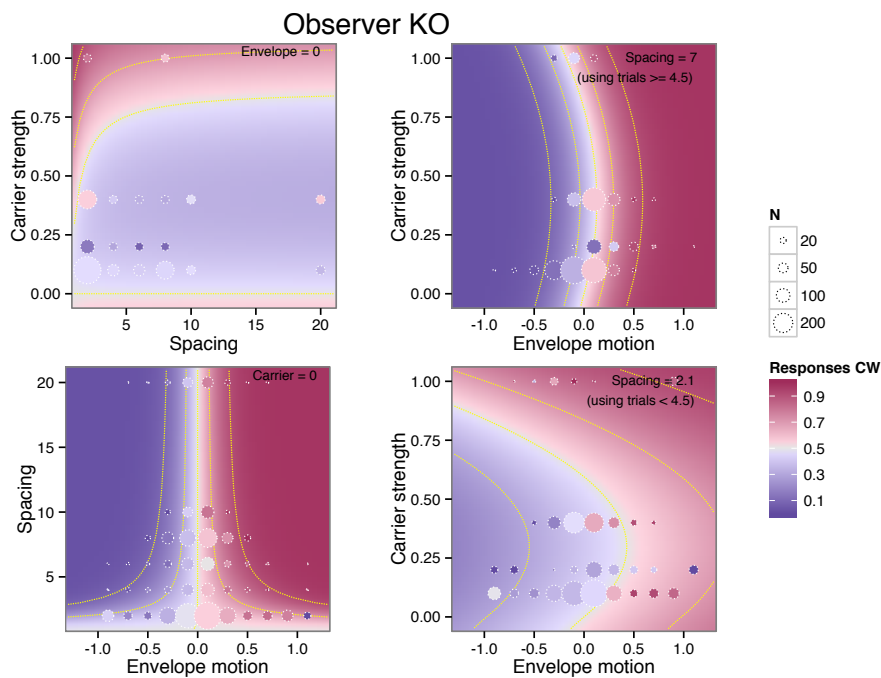


Figure 34: Model fits and summary of data for observer KO. The format of the plot is the same as figure Figure 11.

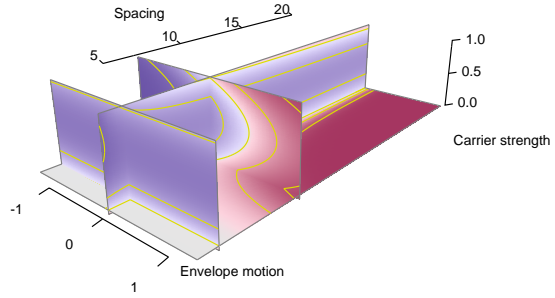


Figure 35: Perspective view of fitted model for observer MC. The format of the plot is the same as figure Figure 10.

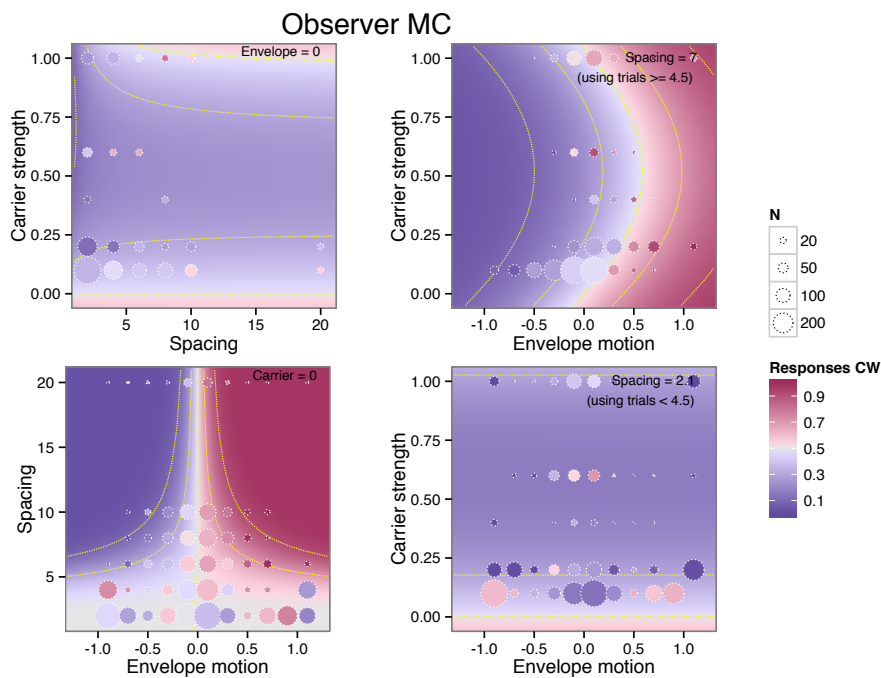


Figure 36: Model fits and summary of data for observer MC. The format of the plot is the same as figure Figure 11.

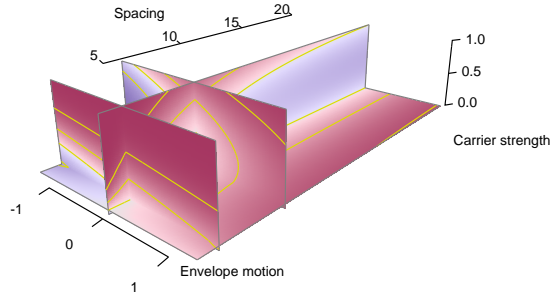


Figure 37: Perspective view of fitted model for observer ML. The format of the plot is the same as figure Figure 10.

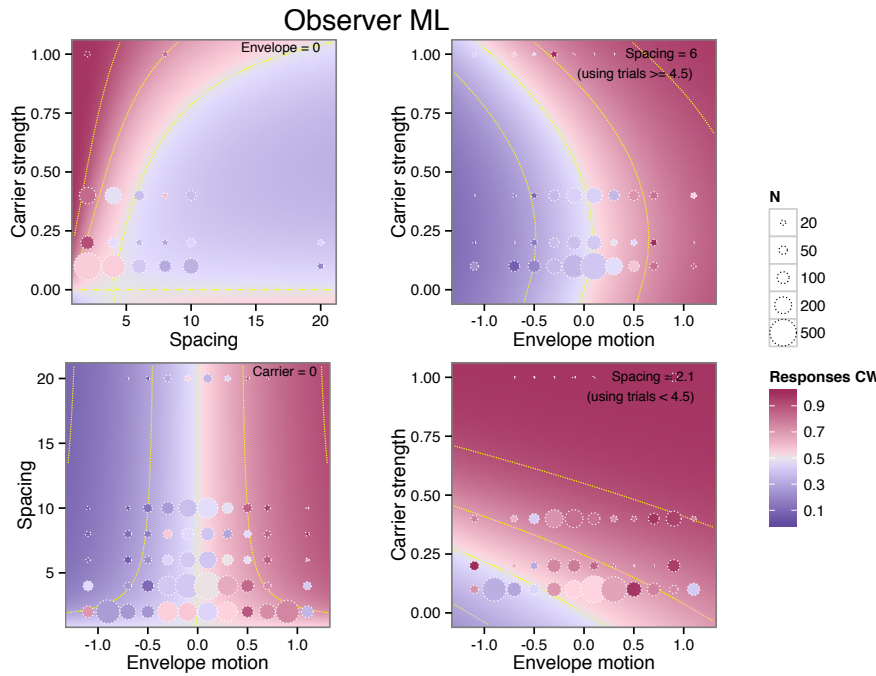


Figure 38: Model fits and summary of data for observer ML. The format of the plot is the same as figure Figure 11.

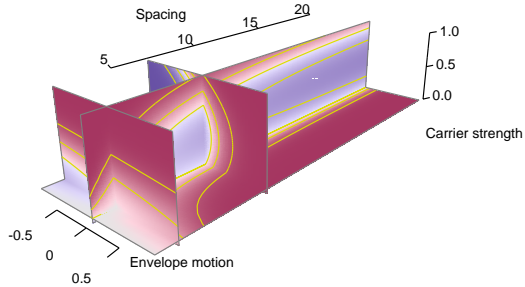


Figure 39: Perspective view of fitted model for observer NJ. The format of the plot is the same as figure Figure 10.

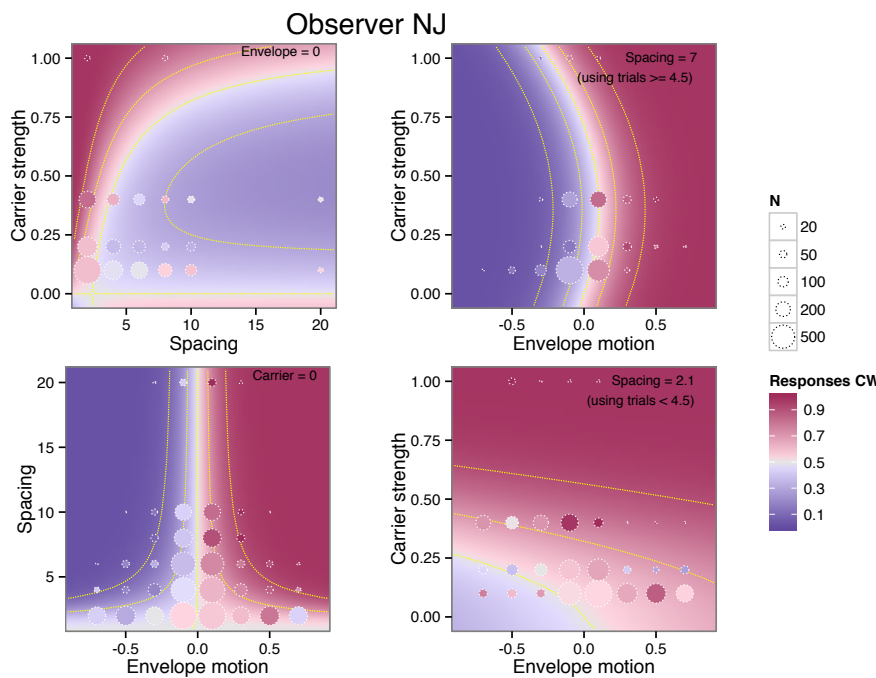


Figure 40: Model fits and summary of data for observer NJ. The format of the plot is the same as figure Figure 11.

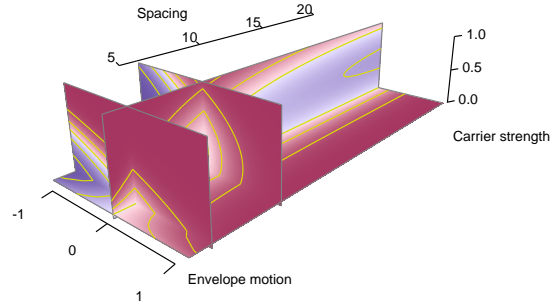


Figure 41: Perspective view of fitted model for observer NS. The format of the plot is the same as figure Figure 10.

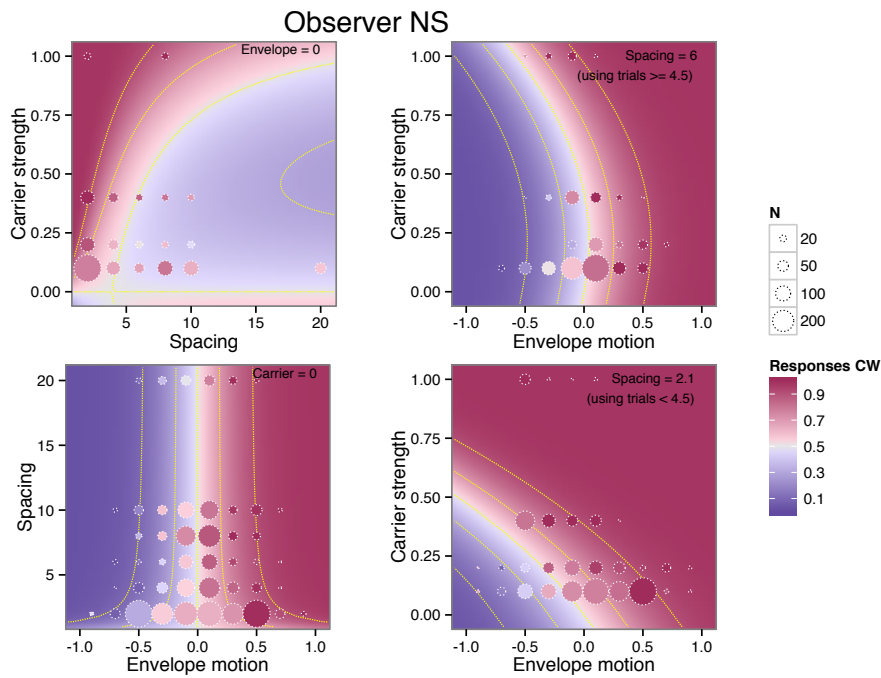


Figure 42: Model fits and summary of data for observer NS. The format of the plot is the same as figure Figure 11.

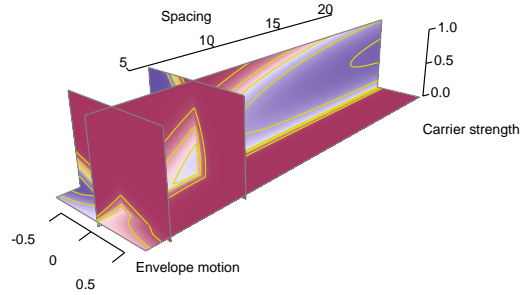


Figure 43: Perspective view of fitted model for observer PBM. The format of the plot is the same as figure Figure 10.

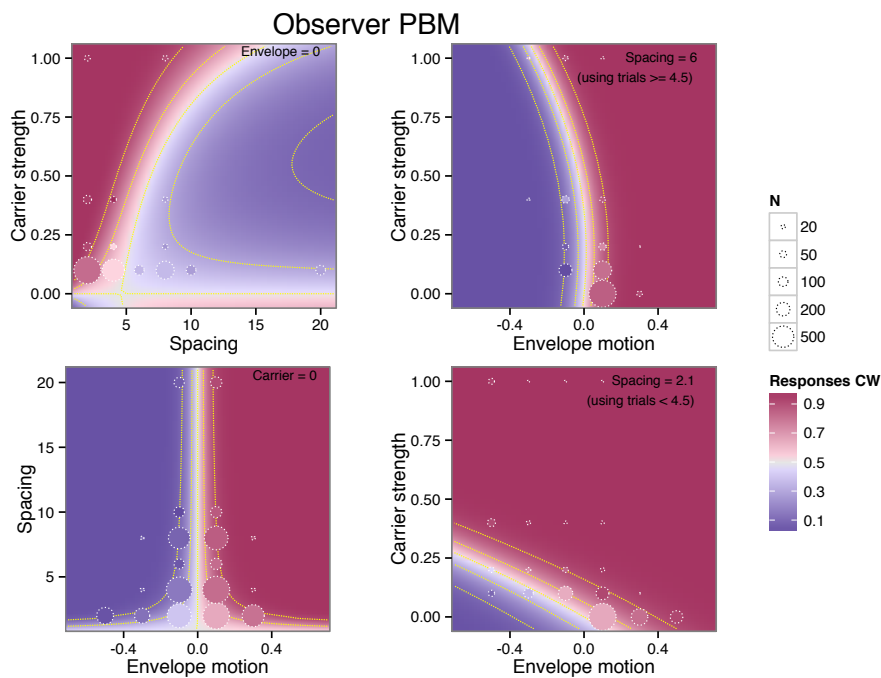


Figure 44: Model fits and summary of data for observer PBM. The format of the plot is the same as figure Figure 11.

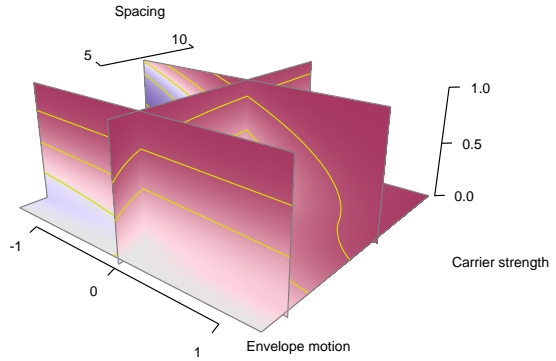


Figure 45: Perspective view of fitted model for observer TL. The format of the plot is the same as figure Figure 10.

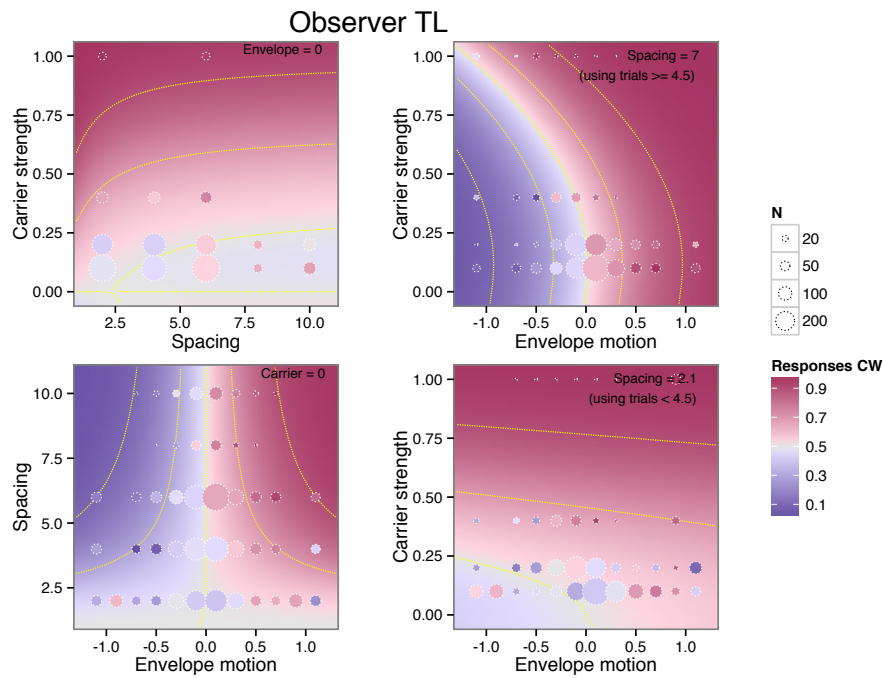


Figure 46: Model fits and summary of data for observer TL. The format of the plot is the same as figure Figure 11.

10.2 Sensitivity to envelope displacement

Figure [Figure 47](#) depicts the sensitivity measure $\beta_{\Delta x}(S)$ as a function of spacing. The construction of the measure and the figure is the same as described in [With shorter distances between elements, sensitivity to envelope motion declines.](#)

10.3 Sensitivity to carrier motion

Figure [Figure 48](#) measures the spacing-dependent summation of carrier motion, denoted in the model as M_S for all observers who participated in the experiment. The construction is described in section [§ 5.2.2](#).

10.4 Carrier repulsion

Figure [Figure 48](#) depicts the repulsion to carrier motion M_I for all observers who participated in the experiment. The construction is described in section [§ 5.4.4](#).

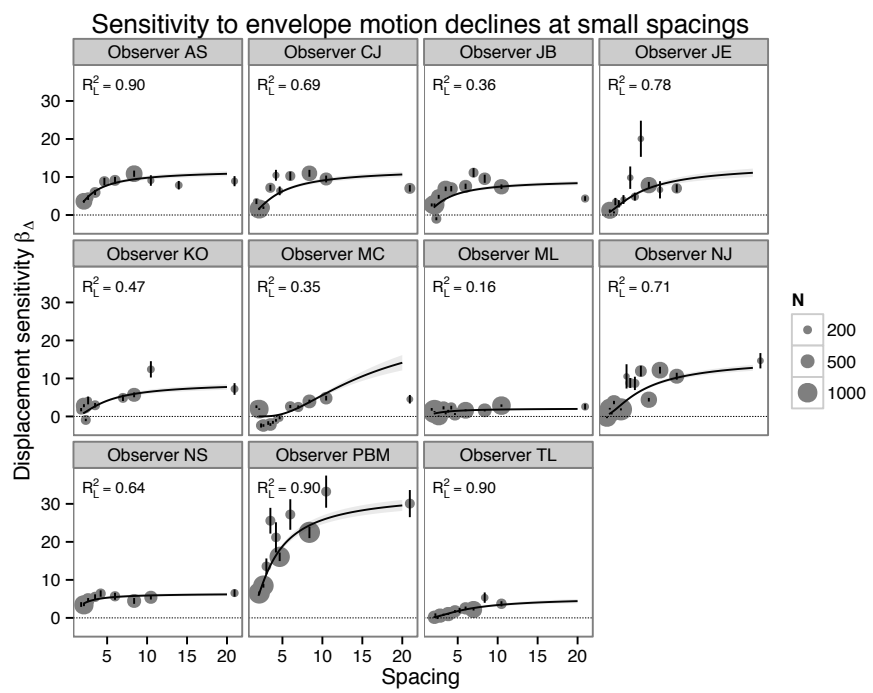


Figure 47: Sensitivity to envelope motion as a function of element spacing. This is a complete version of figure Figure 12 showing all observers, and is otherwise formatted identically.

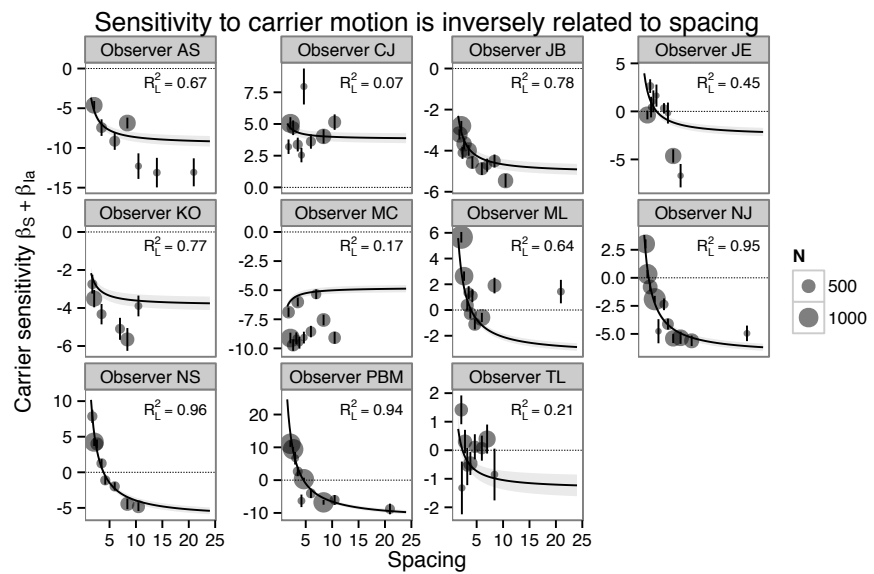


Figure 48: Sensitivity to carrier motion as a function of spacing. This is a complete version of Figure 13 showing all observers; see § 5.2.2 for details on construction.

```
## %^%%-%%^+%%call%%v%abs.pmaxabs.pminadd_energiesadd_predictionsalterappend_arrowsasisifyas
```

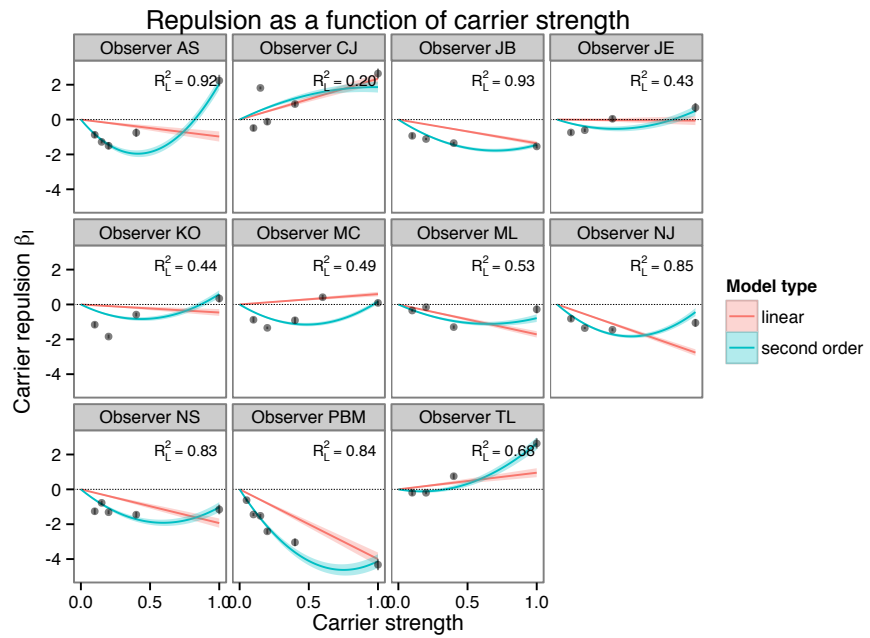


Figure 49: The strength of the repulsion effect as a function of carrier strength. This is a version of Figure 14 showing all observers; see § 5.4.5 for details on construction.

References

- Adelson, E. H. and Bergen, J. R. (1985). Spatiotemporal energy models for the perception of motion. *J Opt Soc Am A*, 2(2):284–299.
- Adelson, E. H. and Movshon, J. A. (1982). Phenomenal coherence of moving visual patterns. *Nature*, 300(5892):523–525.
- Akaike, H. (1974). A new look at the statistical model identification. *Automatic Control, IEEE Transactions on*, 19(6):716–723.
- Anderson, S. J. and Burr, D. C. (1987). Receptive field size of human motion detection units. *Vision Res*, 27(4):621–35.
- Anderson, S. J. and Burr, D. C. (1989). Receptive field properties of human motion detector units inferred from spatial frequency masking. *Vision Res*, 29(10):1343–58.
- Anderson, S. J. and Burr, D. C. (1991). Spatial summation properties of directionally selective mechanisms in human vision. *J Opt Soc Am A*, 8(8):1330–9.
- Anderson, S. J., Burr, D. C., and Morrone, M. C. (1991). Two-dimensional spatial and spatial-frequency selectivity of motion-sensitive mechanisms in human vision. *J Opt Soc Am A*, 8(8):1340–51.
- Anstis, S. and Kim, J. (2011). Local versus global perception of ambiguous motion displays. *J Vis*, 11(3):13.
- Anstis, S. M. (1970). Phi movement as a subtraction process. *Vision Res*, 10(12):1411–30.
- Anstis, S. M. and Cavanagh, P. (1981). What goes up need not come down: Moving flickering edges give positive motion aftereffects. In Long, J. B. and Baddeley, A. D., editors, *Attention and performance IX*, chapter 4, pages 63–78. L. Erlbaum Associates.
- Anstis, S. M. and Rogers, B. J. (1975). Illusory reversal of visual depth and movement during changes of contrast. *Vision Res*, 15:957–61.
- Archer, K. J., Lemeshow, S., and Hosmer, D. W. (2007). Goodness-of-fit tests for logistic regression models when data are collected using a complex sampling design. *Computational Statistics & Data Analysis*, 51(9):4450–4464.
- Banks, M. S., Sekuler, A. B., and Anderson, S. J. (1991). Peripheral spatial vision: limits imposed by optics, photoreceptors, and receptor pooling. *J Opt Soc Am A*, 8(11):1775–87.
- Bex, P. J. and Dakin, S. C. (2002). Comparison of the spatial-frequency selectivity of local and global motion detectors. *J Opt Soc Am A Opt Image Sci Vis*, 19(4):670–7.

- Bex, P. J. and Dakin, S. C. (2005). Spatial interference among moving targets. *Vision Res*, 45(11):1385–1398.
- Bex, P. J., Dakin, S. C., and Simmers, A. J. (2003). The shape and size of crowding for moving targets. *Vision Res*, 43(27):2895–2904.
- Boi, M., Öğmen, H., Krummenacher, J., Otto, T. U., and Herzog, M. H. (2009). A (fascinating) litmus test for human retino- vs. non-retinotopic processing. *J. Vis.*, 9(13):1–11.
- Braddick, O. (1974). A short-range process in apparent motion. *Vision Res*, 14(7):519–27.
- Braddick, O. (1997). Local and global representations of velocity: transparency, opponency, and global direction perception. *Perception*, 26(8):995–1010.
- Brainard, D. (1997). The psychophysics toolbox. *Spatial Vision*, 10(4):433–436.
- Butzer, F., Ilg, U. J., and Zanker, J. M. (1997). Smooth-pursuit eye movements elicited by first-order and second-order motion. *Exp Brain Res*, 115(1):61–70.
- Cassanello, C. R., Edwards, M., Badcock, D. R., and Nishida, S. (2011). No interaction of first- and second-order signals in the extraction of global-motion and optic-flow. *Vision Res*, 51(3):352–61.
- Chen, X., Han, F., Poo, M.-M., and Dan, Y. (2007). Excitatory and suppressive receptive field subunits in awake monkey primary visual cortex (v1). *Proc Natl Acad Sci U S A*, 104(48):19120–5.
- Chubb, C. and Sperling, G. (1988). Drift-balanced random stimuli: a general basis for studying non-fourier motion perception. *J Opt Soc Am A*, 5(11):1986–2007.
- Chubb, C. and Sperling, G. (1989). Two motion perception mechanisms revealed through distance-driven reversal of apparent motion. *Proc Natl Acad Sci U S A*, 86(8):2985–2989.
- Collett, D. (2003). *Modelling binary data*. Texts in statistical science. Chapman & Hall/CRC, Boca Raton, 2nd ed edition.
- Cornelissen, F. W., Peters, E. M., and Palmer, J. (2002). The eyelink toolbox: eye tracking with matlab and the psychophysics toolbox. *Behav Res Methods Instrum Comput*, 34(4):613–617.
- Cropper, S. J. (2001). Local and global motion signals and their interaction in space and time. In Zanker, J. M. and Zeil, J., editors, *Motion Vision - Computational, Neural, and Ecological Constraints*. Springer Verlag, Berlin Heidelberg New York.
- De Valois, R. L. and De Valois, K. K. (1991). Vernier acuity with stationary moving gabor. *Vision Research*, 31(9):1619–1626.

- Derrington, A. M. and Badcock, D. R. (1985). Separate detectors for simple and complex grating patterns? *Vision Res*, 25(12):1869–78.
- Edwards, M. and Badcock, D. R. (1995). Global motion perception: no interaction between the first- and second-order motion pathways. *Vision Res*, 35(18):2589–602.
- Feng, C., Jiang, Y., and He, S. (2007). Horizontal and vertical asymmetry in visual spatial crowding effects. *J Vis*, 7(2):13.1–10.
- Graham, N. V. (2011). Beyond multiple pattern analyzers modeled as linear filters (as classical v1 simple cells): useful additions of the last 25 years. *Vision Res*, 51(13):1397–430.
- Hawken, M. J. and Gegenfurtner, K. R. (2001). Pursuit eye movements to second-order motion targets. *J Opt Soc Am A Opt Image Sci Vis*, 18(9):2282–2296.
- Hedges, J. H., Gartshteyn, Y., Kohn, A., Rust, N. C., Shadlen, M. N., Newsome, W. T., and Movshon, J. A. (2011). Dissociation of neuronal and psychophysical responses to local and global motion. *Curr Biol*, 21(23):2023–8.
- Hosmer, D. W., Lemeshow, S., and Sturdivant, R. X. (2013). *Applied logistic regression*. Wiley series in probability and statistics. Hoboken, NJ: Wiley, third edition.
- Ilg, U. J. and Churan, J. (2004). Motion perception without explicit activity in areas mt and mst. *Journal of Neurophysiology*, 92(3):1512–1523.
- Illdreth, E. C. and Ullman, S. (1982). The measurement of visual motion. Technical report, Massachusetts Institute of Technology. A.I. Memo No. 699.
- Kiani, R., Hanks, T. D., and Shadlen, M. N. (2008). Bounded integration in parietal cortex underlies decisions even when viewing duration is dictated by the environment. *J Neurosci*, 28(12):3017–29.
- Klein, S. A. and Levi, D. M. (1985). Hyperacuity thresholds of 1 sec: theoretical predictions and empirical validation. *J Opt Soc Am A*, 2(7):1170–1190.
- Levi, D. M. (2008). Crowding—an essential bottleneck for object recognition: a mini-review. *Vision Res*, 48(5):635–654.
- Levi, D. M., Klein, S. A., and Hariharan, S. (2002). Suppressive and facilitatory spatial interactions in foveal vision: foveal crowding is simple contrast masking. *J Vis*, 2(2):140–166.
- Lindner, A. and Ilg, U. J. (2000). Initiation of smooth-pursuit eye movements to first-order and second-order motion stimuli. *Exp Brain Res*, 133(4):450–6.
- Livingstone, M. S., Pack, C. C., and Born, R. T. (2001). Two-dimensional substructure of mt receptive fields. *Neuron*, 30(3):781–93.

- Lu, Z. L. and Sperling, G. (1995). The functional architecture of human visual motion perception. *Vision Res*, 35(19):2697–2722.
- Lu, Z. L. and Sperling, G. (2001). Three-systems theory of human visual motion perception: review and update. *J Opt Soc Am A Opt Image Sci Vis*, 18(9):2331–2370.
- Majaj, N. J., Carandini, M., and Movshon, J. A. (2007). Motion integration by neurons in macaque mt is local, not global. *J Neurosci*, 27(2):366–70.
- Mareschal, I., Morgan, M. J., and Solomon, J. A. (2010). Cortical distance determines whether flankers cause crowding or the tilt illusion. *J Vis*, 10(8):13.
- Mather, G., Cavanagh, P., and Anstis, S. M. (1985). A moving display which opposes short-range and long-range signals. *Perception*, 14(2):163–166.
- Mather, G. and Pavan, A. (2009). Motion-induced position shifts occur after motion integration. *Vision Res*, 49(23):2741–6.
- McGraw, P. V., Walsh, V., and Barrett, B. T. (2004). Motion-sensitive neurones in v5/mt modulate perceived spatial position. *Curr Biol*, 14(12):1090–3.
- Meilstrup, P. B. and Shadlen, M. N. (2008). Integration of local and global visual motion revealed by localization judgments. Program No. 460.11/GG3. In *2008 Neuroscience Meeting Planner*. Washington, DC: Society for Neuroscience. Online.
- Movshon, J. A., Adelson, E. H., Gizzi, M. S., and Newsome, W. T. (1985). The analysis of moving visual patterns. In Chagas, C., Gattass, R., and Gross, C., editors, *Pattern Recognition Mechanisms*. Rome: Vatican Press.
- Movshon, J. A. and Newsome, W. T. (1996). Visual response properties of striate cortical neurons projecting to area mt in macaque monkeys. *J Neurosci*, 16(23):7733–41.
- Movshon, J. A., Thompson, I. D., and Tolhurst, D. J. (1978). Receptive field organization of complex cells in the cat's striate cortex. *Journal of Physiology*, 283:79–99.
- Newsome, W. T., Britten, K. H., and Movshon, J. A. (1989). Neuronal correlates of a perceptual decision. *Nature*, 341(6237):52–4.
- Nishida, S. (2011). Advancement of motion psychophysics: review 2001-2010. *J Vis*, 11(5):11.
- Nishida, S. and Johnston, A. (1999). Influence of motion signals on the perceived position of spatial pattern. *Nature*, 397(6720):610–2.
- Nishida, S., Ledgeway, T., and Edwards, M. (1997). Dual multiple-scale processing for motion in the human visual system. *Vision Res*, 37(19):2685–98.

- Nishida, S. and Sato, T. (1992). Positive motion after-effect induced by bandpass-filtered random-dot kinematograms. *Vision Res*, 32(9):1635–46.
- Pelli, D. and Tillman, K. (2008). The uncrowded window of object recognition. *Nat Neurosci*, pages 1129–1135.
- Pelli, D. G. (2008). Crowding: a cortical constraint on object recognition. *Curr Opin Neurobiol*, 18(4):445–451.
- Ramachandran, V. S. and Anstis, S. M. (1990). Illusory displacement of equiluminous kinetic edges. *Perception*, 19(5):611–6.
- Rashbass, C. (1961). The relationship between saccadic and smooth tracking eye movements. *Journal of Physiology*, 159:326–338.
- Rust, N. C., Mante, V., Simoncelli, E. P., and Movshon, J. A. (2006). How mt cells analyze the motion of visual patterns. *Nature Neuroscience*, 9(11):1421–1431.
- Rust, N. C., Schwartz, O., Movshon, J. A., and Simoncelli, E. P. (2005). Spatiotemporal elements of macaque v1 receptive fields. *Neuron*, 46(6):945–956.
- Sekuler, R. (1996). Motion perception: a modern view of wertheimer's 1912 monograph. *Perception*, 25(10):1243–1258.
- Shadlen, M. N., Zohary, E., Britten, K. H., and Newsome, W. T. (1993). Directional properties of MT neurons examined with motion energy filtered apparent motion stimuli. *Investigataive Ophthalmology and Visual Science Supplement*, 34(4):908.
- Shapiro, A., Lu, Z.-L., Huang, C.-B., Knight, E., and Ennis, R. (2010). Transitions between central and peripheral vision create spatial/temporal distortions: a hypothesis concerning the perceived break of the curveball. *PLoS One*, 5(10):e13296.
- Shapiro, A., Lu, Z.-L., Knight, E., and Ennis, R. (2009). The break of the curveball. In *Best Illusion of the Year Contest*. Neural Correlate Society. <http://illusionoftheyear.com/2009/the-break-of-the-curveball/>.
- Shapiro, A. G. (2008). Feature blur in peripheral vision. Program No. 811.3. In *2008 Neuroscience Meeting Planner*. Washington, DC: Society for Neuroscience. Online.
- Shapiro, A. G., Knight, E. J., and Lu, Z.-L. (2011). A first- and second-order motion energy analysis of peripheral motion illusions leads to further evidence of "feature blur" in peripheral vision. *PLoS One*, 6(4):e18719.
- Simoncelli, E. P. and Heeger, D. J. (1998). A model of neuronal responses in visual area MT. *Vision Research*, 38(5):743–761.

- Steinman, R. M., Pizlo, Z., and Pizlo, F. J. (2000). Phi is not beta, and why Wertheimer's discovery launched the gestalt revolution. *Vision Research*, 40(17):2257–2264.
- Touryan, J., Felsen, G., and Dan, Y. (2005). Spatial structure of complex cell receptive fields measured with natural images. *Neuron*, 45(5):781–91.
- Tse, P. (2006). The infinite regress illusion. In *Best Illusion of the Year Contest*. Neural Correlate Society. <http://illusionoftheyear.com/2006/infinite-regress-illusion/>.
- Tse, P. U. and Hsieh, P. J. (2006). The infinite regress illusion reveals faulty integration of local and global motion signals. *Vision Research*, 46(22):3881–3885.
- Tsiatis, A. A. (1980). A note on a goodness-of-fit test for the logistic regression model. *Biometrika*, 67(1):250–251.
- Vaina, L. M. and Cowey, A. (1996). Impairment of the perception of second order motion but not first order motion in a patient with unilateral focal brain damage. *Proc Biol Sci*, 263(1374):1225–1232.
- Vaina, L. M. and Soloviev, S. (2004). First-order and second-order motion: neurological evidence for neuroanatomically distinct systems. *Progress in Brain Research*, 144:197–212.
- Virsu, V., Rovamo, J., Laurinen, P., and Näsänen, R. (1982). Temporal contrast sensitivity and cortical magnification. *Vision Res*, 22(9):1211–7.
- von Helmholtz, H. (1925). *Treatise on Physiological Optics*. Electronic edition (2001): University of pennsylvania edition. J. P. C. Southell, Trans. From the 3rd German ed., 1910.
- Watson, A. B. and Ahumada, A. J. (1985). Model of human visual-motion sensing. *Optical Society of America, Journal, A: Optics and Image Science*, 2:322–342.
- Watson, A. B. and Turano, K. (1995). The optimal motion stimulus. *Vision Res*, 35(3):325–336.
- Wertheimer, M. (1912). Experimentelle studien über das sehen von bewegung. *Zeitschrift für Psychologie und Physiologie der Sinnesorgane*, 61:161 – 265.
- Wertheimer, M., Spillmann, L., Sarris, V., and Sekuler, R. (2012). *On perceived motion and figural organization*. MIT Press, Cambridge, Mass.
- Whitney, D. and Levi, D. M. (2011). Visual crowding: a fundamental limit on conscious perception and object recognition. *Trends Cogn Sci*, 15(4):160–8.
- Wichmann, F. A. and Hill, N. J. (2001). The psychometric function: I. fitting, sampling, and goodness of fit. *Percept Psychophys*, 63(8):1293–313.

- Williams, D. W. and Sekuler, R. (1984). Coherent global motion percepts from stochastic local motions. *Vision Res*, 24(1):55–62.
- Wright, M. J. and Johnston, A. (1983). Spatiotemporal contrast sensitivity and visual field locus. *Vision Res*, 23(10):983–9.
- Zanker, J. M. (1990). Theta motion: a new psychophysical paradigm indicating two levels of visual motion perception. *Naturwissenschaften*, 77(5):243–6.
- Zanker, J. M. (1993). Theta motion: a paradoxical stimulus to explore higher order motion extraction. *Vision Res*, 33(4):553–69.
- Zanker, J. M. (1997). Second-order motion perception in the peripheral visual field. *J Opt Soc Am A Opt Image Sci Vis*, 14(7):1385–92.